Unusual morphologies and the occurrence of pseudomorphs after ikaite ($CaCO_3 \bullet 6H_2O$) in fast growing, hyperalkaline speleothem

LP Field[1*], AE Milodowski[1], RP Shaw[1], LA Stevens [2], MR Hall[1,2], A Kilpatrick[1], J Gunn[3], SJ Kemp[1], MA Ellis[1],

[1] British Geological Survey, Environmental Science Centre, Keyworth NG12 5GG, UK

[2] The University of Nottingham, Nottingham Centre for Geomechanics, Faculty of Engineering, University Park, Nottingham, NG7 2RD, UK

[3] The University of Birmingham, Limestone Research Group, School of Geography, Earth and Environmental Sciences, Edgbaston, Birmingham, B15 2TT, UK

*corresponding author. lorfie@bgs.ac.uk

Abstract

Unusual speleothem, associated with hyperalkaline (pH>12) groundwaters have formed within a shallow, abandoned railway tunnel at Peak Dale, Derbyshire, UK. The hyperalkaline groundwaters are produced by the leaching of a thin layer (<2 m) of old lime kiln waste above the soil-bedrock surface above the tunnel by rainwater. This results in a different reaction and chemical process to that more commonly associated with the formation of calcium carbonate speleothems from Ca-HCO_3-type groundwaters and degassing of CO_2. Stalagmites within the Peak Dale tunnel have grown rapidly (averaging 33 mm y^{-1}), following the closure of the tunnel 70 years ago. They have an unusual morphology comprising a central sub-horizontally-laminated column of micro- to nano-crystalline calcium carbonate encompassed by an outer sub-vertical assymetric ripple-laminated layer. The stalagmites are largely composed of secondary calcite forming pseudomorphs (<1 mm) which we believe to be predominantly after the 'cold climate' calcium carbonate polymorph, ikaite (calcium carbonate hexahydrate: $CaCO_3 \bullet 6H_2O$), with minor volumes of small (<5 μm) pseudomorphs after vaterite. The tunnel has a near constant temperature of 8 - 9 ^{o}C which is

slightly above the previously published crystallisation temperatures for ikaite (<6 ^{o}C). Analysis of a stalagmite actively growing at the time of sampling, and preserved immediately within a dry nitrogen cryogenic vessel, indicates that following crystallisation of ikaite, decomposition to calcite occurs rapidly, if not instantaneously. We believe this is the first occurrence of this calcium carbonate polymorph observed within speleothem.

Keywords: ikaite, speleothem, hyperalkaline, calcium carbonate hexahydrate

Introduction

Speleothem have long been established as a valuable dating proxy, recording long-term palaeoclimatic and palaeohydrological conditions on scales of annual to up to a million years or more (e.g. McDermott, 2004, McMillan et al., 2005, Baker et al., 2008, Fairchild and Baker, 2012). Natural speleothem growth is slow, in the order of tens to hundreds of microns per year (Baker et al., 1998) so the resolution of these records is limited. These speleothem are most commonly formed in limestone caves and caverns from Ca^{2+} - HCO_3^- type groundwater, where calcium carbonate (calcite, or less commonly, aragonite) precipitates as a result of outgassing of CO_2 (Equation 1).

$$2Ca^{2+}_{(aq)} + 2HCO^{3-}_{(aq)} \rightarrow CaCO_{3(s)} + CO_{2(g)} + H_2O \qquad \text{[Equation 1]}$$

Calcium carbonate precipitation from hyperalkaline Ca-OH-type groundwater discharging into a cave or tunnel, results from direct absorption and reaction with atmospheric CO_2 (Equation 2).

$$Ca^{2+}_{(aq)} + 2OH^-_{(aq)} + CO_{2(g)} \rightarrow CaCO_{3(s)} + H_2O \qquad \text{[Equation 2]}$$

Hyperalkaline Ca-OH-type groundwaters often occur as a result of anthropogenic processes which alter the landscape, such as industrial lime-kilning processes. This causes a different reaction and chemical process (sometimes referred to as 'concrete carbonation'), to that associated with the formation of the far more common calcium carbonate speleothems (Barnes et al., 1982; Hartland et al., 2010; Pinsent et al., 1956; Sundqvist et al., 2005). At high pH (>9.5), any carbonate species in solution will be dominated by CO_3^{2-} rather than HCO_3^-. Furthermore, the solubility of $CaCO_3$ in these

Ca-OH-type dripwaters is extremely low, and therefore CO_2 is sequestered from the atmosphere, rather than being degassed. (Hartland et al., 2010; Macleod et al., 1991: Newton et al., 2015).

Speleothem growth from these hyperalkaline fluids is rapid, for example up to 10 mm y^{-1} for stalagmites at Poole's Cavern in Derbyshire (Baker et al., 1999), and 100 mm y^{-1} for straw stalactites at the Wujiangdu Hydropower Station, Guizhou, China (Liu and He, 1998), giving potential for higher resolution climate records than speleothem formed by the more conventional CO_2 degassing process.

Calcium carbonate has several polymorphs, varying in stability and crystal system: calcite is the dominant speleothem-forming polymorph, being the most stable, with a trigonal crystal system (Self and Hill, 2003). Aragonite, (orthorhombic) is also a common cave deposit mineral, but it is metastable at Earth surface temperatures and pressures, typically forming speleothem deposits in warm caves (>12 ^{o}C), but also over a range of temperatures from 2.4 ^{o}C in the Columbia Icefields of Alberta, Canada to 20 ^{o}C in Lechuguilla, US. SW (Frisia et al., 2002). Calcite can precipitate simultaneously with aragonite within the same speleothem (e.g. McMillan et al., 2005), but more usually, when both are present, they represent either changing conditions or partial secondary alteration of aragonite to calcite (Railsback et al., 1994). Aragonite can transform slowly to calcite, particularly in a chemically open system, on scales of a thousand years or more (Frisia et al., 2002). Other calcium carbonate polymorphs include vaterite, which is also metastable, but more soluble than aragonite. Vaterite has a hexagonal crystal system and often displays a colloform or spheroidal morphology typical of many metastable minerals. Vaterite has been observed forming as a transition phase between amorphous calcium carbonate (ACC) and calcite (Rodriguez-Blanco et al., 2011).

The hydrous calcium carbonate minerals include the trigonal monohydrocalcite ($CaCO_3 \bullet H_2O$), occasionally found within cave systems as 'cave-ice' or a component of 'moonmilk', and which forms from an Mg-rich amorphous calcium carbonate precursor (Rodriguez-Blanco, et al., 2014). It has also been identified as a significant breakdown product of the hexahydrate ikaite (Dahl and Buchardt, 2006). This rare, cold-climate mineral (calcium carbonate hexahydrate $CaCO_3 \bullet 6H_2O$),

is metastable with respect to both calcite and aragonite and should not exist under the range of pressures and temperatures normally encountered at the Earth's surface (Marland, 1975, Bischoff et al., 1993, Omelon et al., 2000). However the presence of Mg and PO_4 can strongly inhibit calcite crystal growth, and thus promote ikaite stability, (e.g. Bischoff et al., 1993). Ikaite becomes less soluble with decreasing temperature, as opposed to increasing solubility for other calcium carbonate minerals (Omelon, et al., 2000). Ikaite has not to date been reported in any speleothem deposits.

We have been investigating a suite of the less common hyperalkaline spelethem from the perspective of high resolution, single climatic event recording. In the process of evaluating the possibilities, it was necessary to understand the formation of these unusual speleothem. Detailed petrology is not always reported in speleothem studies, and this paper demonstrates the importance of petrographic analysis in order to understand and interpret formation processes and interpretation of climatic implications.

Geological setting and study site

Geological setting

Peak Dale is located within the Carboniferous Bee Low Limestone formation (354 -327 Ma y^{-1}: Waters et al., 2009). These strata, together with the overlying Monsal Dale Limestone Formation form part of the Peak Limestone Group of the Carboniferous Limestone Supergroup (Waters et al., 2009). In this part of the Peak District, (Derbyshire, UK), the Bee Low Limestone Formation comprises principally two limestone members: the Chee Tor Limestone Member and the Miller's Dale Limestone Member, which are separated by the Lower Miller's Dale Lava Member. These limestone units are characterised by highly fractured rock, such that enlargement of the fractures through dissolution predominates over bedding-related karstification (Banks et al., 2009). The Chee Tor Limestone Member was worked for the production of lime in the quarries in the area and forms the host rock to the Peak Dale tunnel.

Study site

The Peak Dale tunnel (53° 17'N, 1° 51'W) is located under a row of terraced houses known as Small Knowle End (formerly Great Rocks Row) in Peak Dale (Figure 1), approximately 5 km NE of the spa town of Buxton, Derbyshire. The tunnel was driven for a quarry spur railway, which linked the Duchy Quarry (a.k.a. Peak Dale Quarry and now a designated Site of Special Scientific Interest (SSSI)) to limekilns alongside the former Midland Railway Company's main-line route between Derby and Manchester. Old lime waste from the local lime-burning industry has been distributed in a thin layer (1-2 m) across the soil and bedrock surface on the land surrounding the houses and gardens of Small Knowle End. The tunnel runs beneath the end of the row of terraced houses, and is located approximately 9 m below the ground level (Figure 1 and 2A). This depth decreases by 2-3 m south-westwards along the length of the tunnel because of the slope of the overlying ground. Access to the tunnel is gained at its northern end through an entrance in the quarry (Figure 2A). The SW end of the tunnel, adjacent to the railway line, is now blocked, leaving an accessible length of ~57 m. The interior of the tunnel comprises 3 zones: the initial 15 m of the tunnel is speleothem free, the central part of the tunnel is a speleothem-rich zone comprising both stalagmites and delicate straw stalactites. The third zone at the rear of the tunnel contains straw stalactites only.

Historical setting

Quarrying within the Peak Dale area has been carried out from at least 1849, with 12 major quarries developing on the eastern side of Buxton, eight of which are in the immediate vicinity of Peak Dale. The Duchy Quarry was active from the 1890s until 1946 (Gagen, 1988; Gagen and Gunn, 1988). Historical Ordnance Survey maps reveal that kilns were located close to railway lines, with thirteen kilns being marked on the 1882 map of Peak Dale (Ordnance Survey, 2013). The majority were sited on the land between Small Knowle End and the Midland Railway line, with the rest sited north of the Peak Dale Tunnel. Lime waste was tipped within close proximity to the kilns, and waste is still in evidence on the land directly above the tunnel between the rows of terraced cottages, and on the open land around the tunnel location (Figure 1).

Materials and methods

Groundwater sampling and analysis

Alkaline groundwater was sampled from dripping seeps in the roof of the tunnel within the main zone of alkaline groundwater inflow. The water was collected in clean polythene bags, held open and strapped over the tops of the main actively-growing stalagmites. The drips were collected over a period of about 1-2 hours, depending on the flow rate, which was more rapid after periods of heavy rainfall. The pH, temperature and electrical conductivity of the water were measured on-site using a portable multi-probe meter (HANNA HI982) with specific electrodes, calibrated for pH using buffer solutions of pH4, pH7 and pH10.

Samples were also taken for chemical analysis, being filtered on-site through 0.2 µm Acrodisc® disposable nylon filter cartridges and stored in 30 ml Nalgene™ LDPE bottles. Sub-samples for cation analysis were preserved by acidification with nitric acid; samples for anion and alkalinity were collected un-acidified but the bottles were filled leaving no headspace. Samples of unfiltered water were also collected for the determination of total dissolved organic carbon. Cations (Ca, Mg, Na, K, Si, Ba, Sr, Mn, Fe, Al, P, S, and selected trace elements) were analysed by inductively-coupled plasma – mass spectrometry (ICP-MS) using an Agilent 7500CX. Anionic species (Cl^-, SO_4^{2-}, NO_3^-, NO_2^-, Br^-, F^- and HPO_4^{2-}) were determined by ion chromatography using a Dionex ICS 5000. The pH and speciated alkalinity (HCO_3^{2-}, CO_3^{2-} and OH^-) were measured by potentiometric titration on a Radiometer TIM 865 TitraLab. Non-particulate organic carbon (NPOC) was also analysed using a Shimadzu TOC V CPH total organic carbon analyser.

Environmental monitoring

The temperature and humidity within the tunnel were monitored using three Lascar Easylog USB 2 data-loggers set up to record every hour. These were installed in the Peak Dale tunnel on the 24th January 2014 and were placed one at each end of the tunnel and a third within the central alkaline groundwater seep discharge zone about 25 m from the tunnel entrance. A conventional minimum-maximum thermometer was installed within the main alkaline groundwater inflow zone,

adjacent to the data-logger. The variation in water level in the tunnel was also recorded during each visit using a plastic rule fixed to one of the stalagmites. Data on external temperature and daily precipitation was obtained for Meteorological Office station 539 at Buxton (UK Meteorological Office, 2014), about 5 km SW from the tunnel.

Speleothem sampling, preparation and analysis

Four samples of stalagmite (identified as MPLT629, MPLT633, MPLT635 and MPLT636) of unknown age were collected from the floor of the central, speleothem-rich zone within Peak Dale tunnel in May 2013. None were in situ, and therefore their exact location, relation to water level during growth, and growth-end dates are unknown. The stalagmite pieces were lying horizontally, and at the time of sampling were entirely submerged. These samples were allowed to dry naturally within the laboratory.

The stalagmite pieces were sectioned along the long axis of growth, and then, because of their extremely fragile nature, the surface of one half was coated in epoxy resin (Epotek 301) to keep it intact, prior to removing a 10 mm slice across the centre of the stalagmite. These slices were then further resin impregnated before photographing and initial analysis. Small amounts of non-resin impregnated material were also mounted onto double-sided adhesive carbon tabs fixed on 10 mm aluminium stubs for morphological analysis by scanning electron microscopy (SEM). Petrographic polished thin sections (~100 μm) were made from two of the initial samples (MPLT629 and MPLT635). These were coated with a thin layer (25 nm) of carbon for high-resolution SEM examination.

In May 2014, an actively-growing speleothem (MPLU683) was removed intact from the rear of the calcified zone and treated as above. The upper 20 mm of an additional, actively-growing stalagmite (MPLU818) was also removed and immediately placed into a liquid-nitrogen-cooled transport shipping container on exit from the tunnel. Following transport the sample was stored in a freezer at -21^{o} C. Small pieces of the frozen sample were removed from the freezer and stored in liquid nitrogen until transferred onto a pre-cooled SEM stage (-5 ^{o}C) for analysis.

Petrographic Analysis

Initial petrographic observations were made optically using a binocular microscope (Olympus SZX-10 Stereomicroscope). Photomicrographs were recorded using an Olympus XC30 high-resolution digital camera attached to the microscope, and processed with Olympus AnalySIS START image software.

Detailed mineralogical and petrographical observations were made on the polished thin sections and mounted stubs using backscattered scanning electron microscopy (BSEM), secondary electron microscopy (SEM) and charge contrast imaging (CCI), using a FEI Company QUANTA 600 environmental scanning electron microscope (ESEM) equipped with an Oxford Instruments INCA Energy 450 energy-dispersive X-ray microanalysis (EDXA) system with a 50 mm^2 Peltier-cooled silicon drift detector (SSD). The ESEM was operated in both variable pressure and conventional high vacuum mode, with electron beam accelerating voltages of 15 and 20 kV respectively. The frozen sample was imaged in full environmental SEM mode (under a water vapour pressure of up to 740 Pa), using a bespoke FEI gaseous secondary electron detector with 100 µm aperture, at a 15 kV electron beam accelerating voltage. The sample was placed on a Peltier-cooled ESEM stage that was pre-cooled to -5 ^{o}C, thereby ensuring the conditions within the ESEM chamber environment were maintained on the water / vapour equilibrium curve in order to keep the sample wet.

Cryogenic X-ray diffraction analysis

Subsamples were removed from various locations within the frozen stalagmite sample (MPLU818), including the upmost, active growth surface. The sampled material was ground to a fine-powder in a chilled, agate pestle and mortar and rinsed with methanol to remove any free water. Once the methanol had evaporated, the powder was then front-loaded into a stainless steel sample holder for analysis.

X-ray diffraction (XRD) analysis was performed using a PANalytical X'Pert Pro series diffractometer equipped with a cobalt-target tube, X'Celerator detector and operated at 45 kV and 40 mA. In order to examine the mineral species in their *in-situ* state, XRD analyses were performed

using a liquid nitrogen-cooled Anton Parr TTK450 chamber attached to the diffractometer system. Samples were examined at a temperature of -20 °C. Following a conditioning period of 30 minutes in the chamber, the random powder mounts were scanned from 4.5-85 °2θ at 2.06 °2θ/minute. Diffraction data were initially analysed using PANalytical X'Pert HighScore Plus version 4.1 software, coupled to the 2014 version of the International Centre for Diffraction Data (ICDD) database.

Porosity and Physisorption

In order to characterise and gain an understanding of the degree of porosity and permeability of the speleothem, porosity and physisorption analysis was carried out. Porosity analysis by mercury intrusion porosimetry (MIP) was performed using a Micromeritics Autopore IV 9500.V1 with a maximum pressure of 60,000 psi enabling the measurement of pore diameters from 360 – 0.003 µm. Irregular sub-samples of approximately 0.2 – 0.3 g were sub-sampled carefully using a scalpel from both the outer and inner columns and placed in a 5 cc solid penetrometer (1 cm^3 internal diameter). All powder residues were removed leaving irregular solid samples. Prior to analysis, the samples were dried in an oven at 40 °C for 8 hours then outgassed on the instrument under high pressure (0.001 psi) for 1 hour. Both low and high pressure analyses were carried out incrementally from 0.5 – 60,000 psi with an equilibration time of 45 seconds per pressure point. The contact angle and surface tension parameters were taken as 140 ° and 0.485 N/m^2, respectively. A blank correction was carried out on the penetrometer under identical analysis conditions and intrusion data subtracted from sample data.

Nitrogen sorption isotherms and textural properties were determined on intact sample at -196 °C using a conventional volumetric technique by a Micrometrics ASAP 2020 gas adsorption instrument. Before analysis, the sub-samples (approximately 0.2 – 0.3 g) were dried at 40 °C for 8 hours in an oven and outgassed under high vacuum (0.0002 psi) at 40 °C for 4 hours. The surface area of the intact materials was determined using the standard gas absorption method, BET (Brunauer et al., 1938) based on adsorption data in the relative pressure (P/P_o) range of 0.05 - 0.35,

and pore volume was calculated from the amount of nitrogen adsorbed at P/P_o of ca. 0.99 spanning micro (<0.002 μm), meso (0.002 – 0.050 μm) and macropore (> 0.050 μm) up to 0.140 μm.

Capillary potential was tested very simply using a half slice of a dry speleothem (280 mm) placed in a container of 260 ml^3 water dosed with food colouring at normal room temperature. The take up and rise of the dyed water through the sample was measured at specific time intervals over an 18 hr period.

Observations and results

Tunnel observations and environmental conditions

Because of its close proximity to the surface, the Peak Dale tunnel environment was observed to rapidly respond to rainfall. As noted above, within the first 15 m of the tunnel there is an absence of speleothem formations, despite frequent drip points; calcium carbonate formations are concentrated within a discrete interval about 30 m long, where hyperalkaline groundwater seeps through a fracture zone in the limestone roof of the tunnel that connects with rainwater percolating through the lime waste above (Figure 2B). At Peak Dale these hyperalkaline groundwaters are produced by the leaching of a thin layer (1-2 m) of lime kiln waste distributed on the ground surface above the tunnel. Rainwater percolating through this lime waste leaches portlandite ($Ca(OH)_2$, formed by the hydration of lime (CaO)), and potentially other clinker phases in the lime waste (such as calcium silicates and aluminates), giving rise to high pH Ca-OH-type groundwaters which discharge through the fracture zone to the tunnel below. Visual evidence of these high pH groundwaters can be seen in the surface environs of Peak Dale Tunnel e.g. hyperalkaline groundwaters draining from lime waste mounds into the Dale Road Brook to the northwest of the Peak Dale tunnel where subaerial precipitation of calcium carbonate is occurring, and similar deposits are forming in the cess alongside the present railway line.

In Peak Dale, stalagmites have grown to heights of ~1.7 m. A photograph of the tunnel interior taken in 1964 by Mr. P. Deakin, shows minimal precipitation indicating that speleothem

growth had only recently been initiated. Therefore, assuming growth began during 1964 (~51 yrs. ago), this suggests a rapid, average growth of around 33 mm y^{-1}. To further demonstrate rapid growth, a tile was placed on top of an active stalagmite in Peak Dale between routine visits. This recorded 12.46 mm of growth in the 32 days between 3rd October and 4th November 2014, representing an exceptionally fast growth rate equivalent to 142 mm y^{-1} (assuming constant growth). Recent studies at nearby Poole's Cavern also found that precipitation rates from dripwaters above pH 11 are significantly more rapid compared to lower pH and non-hyperalkaline dripwaters (Newton et al. 2015).

Water levels on the floor of the tunnel fluctuate (Figure 2C and D) during the year. However the far end of the tunnel is now permanently flooded to a depth of ~1 – 1.5 m, limiting speleothem formation at the rear of the tunnel to straw stalactites only (Figure 2E). Within the first 5 m of the tunnel, water levels have been observed up to ~300 mm above the tunnel floor, but can recede revealing a "beach" area during dry periods. The floor of the tunnel within the main zone of stalagmite formation was only observed partially dry on one occasion during a three year period, in September 2014. Because stalagmites are unable to establish themselves underwater, this indicates that new speleothem formation within the tunnel is limited, and that drainage within the tunnel has altered over time. The southern corner of the nearby Duchy Quarry is also frequently flooded, with fluctuating water levels reflecting seasonal rainfall.

The tunnel is relatively enclosed resulting in a near constant temperature within the tunnel of 8-9 ^{o}C ±0.5 (Figure 3). The data-loggers and the minimum-maximum thermometer all recorded the same consistent temperature range. Relative humidity was recorded as > 80 %.

Groundwater chemistry

The chemistry of groundwater drips collected from straw stalactites and associated with speleothem development within the main hyperalkaline groundwater inflow zone is shown in Table 1. The variation in the major aqueous chemical components over the year from January to November 2014 is also illustrated in Figure 4.

The dripwaters associated with speleothem development in the tunnel are hyperalkaline. For most of the year they are dominated by Ca^{2+}-OH^{-}-type groundwater, and maintain a pH between 12.2 and 12.6 (Table 1, Figure 4). Na, K, Cl^{-}, CO_3^{-2}, SO_4^{2-}, NO_3^{-} and NO_2^{-} are normally only minor components. During this time the air temperature (which will be similar to the dripwater temperature) remains constant at about 8.5 (±0.5) °C. However, being very shallow, the groundwater system has been observed to react rapidly to rainfall events, and this can be seen in the dripwater chemistry. During January 2014, the pH decreased to pH 11.5, and was associated with a change from Ca^{2+}-OH^{-}-dominated groundwater to a Na^{+}-Ca^{2+}-Cl^{-}-OH- groundwater composition accompanied by slight decrease in total dissolved solids (Figure 4). This reflects the dilution of the "background" Ca^{2+} - OH^{-} lime waste leachate by precipitation (snow and rainfall) which had elevated concentrations of sodium and chloride that result from the dissolution of road de-icing salt applied to the overlying road during winter. At other times, the precipitation appears to simply dilute the major cation and anion components with only a slight decrease in pH, as observed in July 2014 (Figure 4), when heavy rain fell 48 hrs prior to sampling. In this case, no enhancement in sodium and chloride was observed following summer rainfall.

Speleothem observations and analysis

General observations

These speleothems are notable for their lack of uniformity and symmetry in their growth. The stalagmites have a slightly convoluted appearance due in part to variations in their width (Figure 5).. Their feedingstraw stalactites also undulate quite considerably along their length, suchthat the position of the drip does not remain constant. Stalagmites also widen when receiving drips from multiple sources which may be time-limited. Gravitational creep of the unconsolidated calcium carbonate during growth is also apparent (Figure 5B), which is generally not observed in speleothem formed by degassing due to their slower precipitation rates resulting in greater crystallinity, and lower water-content. Below the maximum flooding level a distinct euhedral crystallinecoating of secondary calcite has nucleated on the sub-aquerous surface of the stalagmites which contrasts to

the smoother ribbed upper surfaces above the maximum flooding level. On occasions when the drip rate is extremely rapid, a 'splash cup' develops (Allison, 1923) where calcium carbonate precipitate builds up around the drip point creating a central pit (Figure 5C). During periods of slower drip rates, this pit is infilled and the top surface of the speleothem becomes smooth and flat.

Detailed observations

The four initial samples taken from the tunnel yielded two distinctly different morphologies: the two smaller specimens (MPLT629 and MPLT633) comprise a morphology consisting entirely of sub-parallel and sub-horizontal growth laminae similar to the general texture commonly observed in speleothems formed following degassing of CO_2, and also akin to the general texture noted in other hyperalkaline speleothem e.g. Poole's Cavern (e.g. Hartland et al., 2010) and Uppsala (Liu and He, 1998), whereas the two larger specimens (MPLT635 and MPLT636) comprise a thin central column of sub-horizontal laminae encased within vertically-laminated calcium carbonate displaying asymmetric ripple laminae, with their steep slope downwards, indicating deposition from a downward (gravitational) flow along the sides of the stalagmite. Asymmetrical, climbing ripples are a well-documented feature in sedimentary petrography and their formation is well understood (e.g. Tucker, M. 2001). Fairchild and Baker (2012) also note that centimetre scale rippling in stalagmites from Yonderup Cave, Perth, Australia attest to high discharge rates.

Samples MPLT629 and MPLT633 comprise an overall texture of a continuous series of sub-parallel growth laminae. In thin section, truncation and bifurcation of individual laminae is frequent (Figure 6B and C), most likely caused by changes in drip movement and drip rate (Fairchild and Baker, 2012). However, the structure of these hyperalkaline speleothem is more delicate and porous than a speleothem formed by degassing. In thin section, crystals are observed to have nucleated at the base of the laminae, branching outwards during upward growth. Secondary electron (SE) imaging of the stub samples shows that the broader, more porous, banding comprises coarse, upwardly growing crystals with spiral growth morphology, whereas the narrower, denser laminae comprise closely spaced, finer grained, radial clusters (Figure 6D and E). Porosity varies within each

of the laminae, but can be proportionately substantial, being present between individual crystals, their relative branches, and crystal clusters. With continued growth, space becomes limited and crystals grow to fill the remaining interlayer space causing denser bands with minimal pore space (see Figure 6D, E and H). Polarising optical microscopy indicates that some crystals are in optical continuity across several distinct laminae (Figure 6G), showing that (once formed), the crystals acted as nucleation points and continued to grow progressively. The calcite crystals display complex zoning, visible under charge-contrast imaging (CCI) conditions (Figure 6I). No evidence of ikaite precursors (e.g. pseudomorphs or moulds) were identified within these smaller samples.

In contrast, samples MPLT635 and MPLT636 have a far more unusual and complex morphology. These stalagmites comprise a central column of sub-horizontal laminaeencompassed by an outer, sub-vertical ripple-laminated layer, akin to the texture of asymmetrical climbing ripples. Varying fabrics are present between the individual ripples. The most basic ripple type (100-200 µm thick) comprises of a series of laminae displaying unidirectional, outward growing crystals (Figure 7C and E), suggesting growth into a fluid meniscus on the surface of each lamina. However, some laminae also display crystals that have nucleated and grown into void space on both sides of the lamina (Figure 7F). Some colloform calcite growth is present locally which may be pseudomorphs after vaterite, or may represent rapid calcite nucleation from supersaturated solution (Roedder, 1968).

In thin section, the central core comprises sub-horizontal laminae of micro-crystalline calcium carbonate crystals (Figure 8). Within these laminae, features such as slip planes and central pits, created in unconsolidated calcium carbonate sediment during periods of high drip rate (as described above), can be identified. Under the SEM, this central core is seen to comprise rare, dense, sub-horizontal bands of calcium carbonate, but the dominant fabric is a collection of skeletal pseudomorphs (<1 mm: Figure 8A, B and E). These pseudomorphs form hollow moulds (Figure 8C) defined by a layer of skeletal calcite crystals (<10 µm: Figure 8D - I). SEM examination reveals a fresh, euhedral, outer calcite coating around a calcite layer which appears far less pristine (Figure 8H). In

cross section, the outer coating surrounds calcite displaying a skeletal 'cabbage-leaf' texture (Figure 8I).

As samples MPLT635 and MPLT636 were not found in-situ, thin sections from an actively growing stalagmite (MPLU683) were imaged to assess whether or not features identified within samples MPLT635 and MPLT636 were artefacts of being submerged. This actively growing speleothem comprised the same central column and asymmetrical ripples as MPLT635 and 636, and pseudomorphs within the central column are also defined by fine, skeletal calcite crystals, in common with the non in-situ samples.

Small pieces (<5 mm) of frozen material from the top surface of the stalagmites that had been cryogenically preserved on site were imaged under full ESEM conditions. A geometric fabric of moulds up to 1 mm were present (Figure 9E and F), mirroring the textures observed in samples MPLT635 and 636.

Cryogenic X-ray diffraction analysis

Repeated semi-quantitative cryogenic XRD analyses, using the Reference Intensity Ratio (RIR) method, suggest that the sub-samples taken from the stalagmite samples are composed of ~99% calcite and <1% quartz only (Figure 10). This XRD methodology has successfully confirmed the identity of ikaite from a tufa deposit in nearby Harpur Hill (Milodowki et al., 2014 and 2013), although no evidence for the presence of the polymorph ikaite was obtained from these Peak Dale XRD analyses.

Porosity

Nitrogen sorption isotherms of the inner and outer parts of the columns show isotherm shapes indicative of Type IV isotherm, with low adsorption (Figure 11) and hysteresis in the desorption curve. A slight 'knee' in the isotherms can be observed at approximately 0.1 P/P_o showing low micro pore volume, with adsorption rising indicating multilayer adsorption filling mesopores towards capillary condensation at higher relative pressures. BET 'C' constants greater than 10 (Table 2) suggest that porosity does exist within both the micropore (<2 nm dia.) and mesopore (2-50 nm

dia.) ranges. However, during an N_2 BET test it should be noted that the pore volume is only partially filled. This is because we only need to complete a monolayer of adsorbed gas molecules along the pore walls. During BET experiments a pore volume of 0.015 $cm^3\ g^{-1}$ was obtained for the inner column region (1.37% porosity), and low BET specific surface areas of 2.26 $m^2\ g^{-1}$. For the outer columns region 1.27% porosity was obtained and between 0.005 $cm^3\ g^{-1}$ and 0.5271 $m^2\ g^{-1}$. Furthermore, the isotherms show significant adsorption above 0.90 P/P_o indicating that most of the pore volume may be within the macro pore range (>50 nm dia.), much of which is outside the range detectable by analysis of nitrogen sorption isotherms i.e. > 0.140 µm dia. Results from MIP confirmed that most of the pore volume is within the macro pore range (Figure 12). It can be easily seen from cumulative intrusion versus pore size diameter curve in Figure 12 that the inner column region has greater intrusion volume (pore volume) than the outer region, and from Table 2 approximately 3 times greater (1.098 inner, and 0.395 $cm^3\ g^{-1}$ outer). As a consequence, the inner column has a greater pore area than the outer column (21.843 compared to 8.433 $m^2\ g^{-1}$). The inner column has intrusion/pore volume associated with inter-particulate void space spanning 390 – 25 µm, with intrusion increasing from 25 – 10 µm as the mercury enter the pores. Most intrusion occurs within this size range suggesting most pore volume for the inner column is within this size range, further intrusion occurs at lower pore sizes but with less volume. As for the outer column, intrusion occurs at approximately 20 µm without any inter-particulate void space and intrusion increasing to 8 µm. Intrusion of mercury into lower pore sizes is very small, indicating most pore volume for the outer column is restricted to 20 – 8 µm. The pore size diameter versus cumulative pore volume can be split into pore ranges to determine associated pore volumes (Table 3).

Both the inner and outer column has most of their pore volume within the 25 – 10 µm size range, with pore volumes decreasing with pore size. The inner column has a greater pore area as a result of having more pore volume especially in the lower pore size distribution range (< 0.700 µm). Therefore, the outer column has less pore volume but greater mass due to having a high bulk and skeletal density (1.141 and 2.211 g cm^{-3}) and ultimately less % porosity (48 % compared to 64 %).

Results from the capillary test showed an initial rapid take-up of fluid; within 20 minutes the dyed water had risen to a height of 100 mm. Leaving the test overnight (18 hrs), resulted in the full 280 mm section becoming damp, with 215 mL of fluid either being taken up into the speleothem or lost through evaporation.

Discussion

The Peak Dale hyperalkaline stalagmites display very complex growth fabrics. A key feature of the stalagmites is the development of highly microporous laminae that preserve a strongly idiomorphic skeletal fabric (e.g. Figure 8B, C, E). These skeletal fabrics (Figure 8A, B and E) are themselves defined by the aggregation of numerous, calcite crystals which are substantially finer-grained (<10 μm) than the cavities which they are defining (Figure 8C, D, H, F and I). Thus this skeletal fabric appears to represent mouldic cavities produced by the dissolution of a euhedral crystalline precursor phase: the fine-grained calcite would have had to have nucleated on a pre-existing surface in order to form the larger scale forms which are now observed (simple cartoon of the proposed process is provided in Figure 13).

XRD analysis of cryogenically-preserved material taken from the top of an actively-growing stalagmite shows that this skeletal material is composed almost entirely of calcite (~99 weight %). However, the morphology of these moulds is inconsistent with cavities which would have been created by dissolution of euhedral trigonal calcite crystals, but instead displays a habit compatible to monoclinic symmetry. Ikaite ($CaCO_3 \bullet 6H_2O$) is the only monoclinic crystal form of calcium carbonate (Gaines et al., 1997). Recent experimental work by Sánchez-Pastor et al., (2016) also displays ikaite crystals with a monoclinic habit, with individual crystals displaying a remarkable resemblance to the Peak Dale crystals (compare Figure 1a in Sánchez-Pastor et al., (2016), with Figure 9A herein). Transformation of ikaite to calcite will result in a 68% volume change (Shaikh and Shearman, 1987), which would explain the development of the highly porous fabric found in these unusual hyperalkaline speleothem deposits (Figure 13D). Quaternary 'jarrowite' pseudomorphs (now

attributed to ikaite) from NE England have porosities of up to 69%. Shaikh and Shearman (1987) indicate that in their ikaite – vaterite experiments, shape was preserved with an absence of moulds, indicating a piecemeal transformation with concomitant precipitation of vaterite. In the Peak Dale example the moulds have been perfectly preserved, suggesting rapid transformation which may not have involved an interim crystal phase between the precursor and calcite (Figure 13 D). Recent experimental work by Sánchez- Pastor et al., (2016) also shows that ikaite directly transforms into calcite at a temperature of 10 ^{o}C; at 20 ^{o}C this process involves an interim step with the formation of intermediate metastable vaterite.

Ikaite, known to be the cold climate polymorph of calcium carbonate, has been identified precipitating in natural cold-climate environments at temperatures between -1.9 and 4 ^{o}C (e.g. Bischoff et al., 1993; Hansen et al., 2011; Pauly, 1963; Shearman et al., 1989). Experimentally ikaite has been shown to be metastable with respect to the anhydrous calcium carbonates (calcite and aragonite) in the presence of liquid water, and it should not be persistent at temperatures and pressures normally encountered at the Earth's surface (Bischoff et al., 1993; Marland, 1975). Although it is argued in the literature that ikaite decomposes at temperatures above 6-7 ^{o}C (Hansen et al., 2011), ikaite has recently been observed crystallising during cold weather in hyperalkaline spring-water (of similar composition to Peak Dale dripwaters), associated with the leaching of another old lime waste site at Harpur Hill near Buxton (Milodowski et al., 2014 and 2013: see Figure 9D,G, H and I). Harpur Hill lies <7 km south west of Peak Dale at a similar elevation (~350 m). Milodowski et al. (2014) have recently demonstrated that ikaite can crystallise as a metastable phase from hyperalkaline Ca^{2+}-OH^{-}-type groundwater at temperatures up to 10 °C, either through turbulent flow of constant high pH waters causing mixing of water with air and reaction with atmospheric CO_2, or by mixing of the hyperalkaline water with bicarbonate-type groundwater. Ikaite formation has also recently been reported in a man-made environmental setting (an artificial concrete lining of a water channel) in Austria (Boch et al., 2015). Boch et al., (2015) show that ikaite formation is caused

by portlandite dissolution from the concrete resulting in supersaturation with respect of ikaite through instantaneous absorption of atmospheric CO_2.

Previous research suggests that under low-temperature supersaturated conditions, ikaite formation is kinetically favoured by high alkalinity, magnesium and phosphorus, which inhibit the formation of the more stable anhydrous calcium carbonate polymorphs (Bischoff et al., 1993; House, 1987; Buchardt et al., 1997; Ito, 1998; De Lurio and Frakes, 1999; Spielhagen and Tripati, 2009; Hu et al., 2014). However, phosphorus and magnesium are only present in very low concentrations in both the groundwaters at Harpur Hill and in Peak Dale tunnel, and Milodowski et al. (2013 and 2014) concluded that the metastable ikaite formation at Harpur Hill is principally promoted by achieving rapid supersaturation of calcium carbonate, coupled with cold temperature (<10 °C) and the exceptionally highly alkaline portlandite -buffered, pH of the lime waste leachate (pH 12-12.5).

By analogy with Harpur Hill (Milodowski et al., 2014 and 2013)), it seems highly feasible that ikaite could also precipitate from the hyperalkaline dripwaters in the Peak Dale Tunnel, through absorption and reaction with atmospheric CO_2 (Equation 2). The dripwaters have a similar Ca^{2+}-OH^{-} dominated chemistry, with very high pH between pH 12.2 – 12.6 for much of the year (Table 1). The air temperature in the tunnel has a very narrow range (8.5 ±0.5 °C), which is also below the upper temperature limit (~10 °C) of ikaite metastability observed at Harpur Hill. Ikaite persists during cold weather at Harpur Hill because the large volume and supply of hyperalkaline leachate means that, despite its reaction with atmospheric CO_2, there is always an excess of $Ca(OH)_2$ in solution and the pH of the water is effectively buffered at a pH >12. However, in the case of the slower-flowing dripwaters in the Peak Dale tunnel, the finite mass of $Ca(OH)_2$ in solution in each drip is very small relative to the rate of uptake of atmospheric CO_2 (i.e. Peak Dale is an air dominated system). Therefore, we propose that whilst ikaite initially forms on top of the stalagmite as soon as each drip falls, the pH in the splash water rapidly decreases as the $Ca(OH)_2$ in solution is consumed by rapid

reaction with atmospheric CO_2 (Figure 13 A-B). Consequently, ikaite stability will drop rapidly re-dissolving as the pH falls, and calcite will then precipitate as its saturation is reached (Figure 13 C-D).

The hypothesis that ikaite might initially form from the hyperalkaline dripwaters in the Peak Dale tunnel was tested using the PHREEQC modelling package (Parkhurst and Appelo, 2013), supplemented with solubility data for ikaite based on experimental data from Bischoff et al. (1993), and these data are summarised in Table 4.

Saturation indices were initially calculated for the measured fluid compositions (including pH and alkalinity). Saturation indices were then recalculated assuming full equilibrium with atmospheric partial pressure of carbon dioxide (pCO_2 of 0.000400 atm).

Conceptually, this model can be considered as equivalent to emergence of (the analysed) dripwater into the cavern, followed by full equilibration with atmospheric CO_2 during its migration to the cavern floor and initial contact with the speleothem. Individual drips are small and, upon contact with the speleothem, will present a relatively large surface area to the atmosphere, such that we may reasonably assume full equilibrium with the cavern pCO_2 on the order of a few seconds (Newton, 2015). Carbon dioxide partial pressures within such caverns are often elevated, and so an atmospheric pCO_2 may be considered a conservative estimate for the CO_2 concentration in the cavern.

Solubility modelling of the initial dripwater chemistry shows that inflows in January and March 2014 (Table 4) are undersaturated with respect to both ikaite and calcite Later in the year (May to November), the dripwaters are oversaturated with respect to calcite (i.e. positive saturation indices) but only just saturated with respect to ikaite (Table 4). Following equilibration with an atmospheric pCO_2, the modelled saturation indices show that both calcite and ikaite were undersaturated in January 2014, when (as discussed earlier) there was significant dilution of the hyperalkaline leachate following heavy rain and snow fall. However, with the exception of the July 2014 data, both ikaite and calcite are predicted to have been saturated in the dripwaters sampled later that year following equilibration with atmospheric CO_2 (Table 4). The July sample was taken

following a period of heavy rainfall, and measured alkalinity is relatively low in this sample. Hence during equilibration with atmospheric CO_2, pH is not strongly buffered and carbonate saturation indices show a concomitant fall.

These results demonstrate that both ikaite and calcite can feasibly precipitate from the hyperalkaline dripwaters in the Peak Dale tunnel. However, as discussed earlier, previous studies of ikaite have shown that cold conditions and high alkalinity kinetically favour the nucleation of the metastable ikaite in preference to calcite. In this case, it appears that emergent dripwater is, or is close to being, saturated with respect to ikaite. Sorption of CO_2 from the tunnel atmosphere will cause the fluid to become strongly supersaturated with respect to ikaite (as well as calcite), allowing relatively rapid precipitation of the metastable, but kinetically favoured, ikaite. The temperature of the tunnel (8.5 ±0.5 °C) is well within the temperature limits observed for confirmed ikaite formation in similar hyperalkaline lime waste leachate at Harpur Hill (cf. Milodowski et al., (2013 and 2014)).

The reason that the ikaite does not persist in the Peak Dale tunnel speleothem (unlike at nearby Harpur Hill) could be that the pH of the film of dripwater continues to decrease as $Ca(OH)_2$ is depleted through continued absorption of CO_2 from the atmosphere and calcium carbonate precipitation. In the Harpur Hill scenario, the supply of $Ca(OH)_2$ in the extensive hyperalkaline plume is effectively continuous and “infinite” with respect to the relatively small amount of atmospheric CO_2. In that system, pH can be maintained at high values (>pH 12) and is buffered close to portlandite ($Ca(OH)_2$) saturation. However, in the case of the Peak Dale tunnel, each small drop of dripwater represents only a very limited mass of $Ca(OH)_2$, which is small in comparison to the amount of CO_2 available in the atmosphere (resulting in an air-dominated system). Consequently, the pH of each isolated drip is not maintainedclose to portlandite saturation, and falls as reaction with CO_2 proceeds. As the alkalinity is reduced, the fluid will become undersaturated with respect to ikaite before calcite undersaturation is reached. We may hypothesise that under these conditions the ikaite will re-dissolve and calcite precipitate.

As discussed above, these hyperalkaline speleothems exhibit considerable macroporosity (as defined by IUPAC: >50 nm diameter). However, the porosity is distributed in an organised manner that is closely related to differences in the growth structure of the speleothem. From nitrogen sorption and MIP analysis, the central column has approximately 3 times more connected pore volume than the outer; the bulk of the connected pore volume in both sections is within the 25 – 10 μm range. The outer part of the stalagmite column has lower apparent porosity and thus a higher skeletal density than the central column. As discussed earlier, the high porosity within the central part of the column can be explained in part by the initial precipitation of a metastable calcium carbonate phase with high molar volume, such as ikaite, which re-dissolves in the residual dripwater as the pH decreases (as a result of chemisorption of atmospheric CO_2), with calcium carbonate simultaneously re-precipitated as lower molar-volume calcite.

Towards the lateral margins of the large stalagmites the microstructure changes significantly, with the prominent development of denser vertical layers displaying asymmetric ripple lamination. The ripple lamination (with steep ripple faces downwards) is consistent with carbonate film formation along the surface of liquid flowing down the sides of the stalagmites (deposition occurring within a current regime). Here the process of carbonate accretion is markedly different to that which occurs at the top of the stalagmite. We propose that following the initial splashing of the dripwater and rapid precipitation of calcium carbonate on the top of the stalagmite, the excess water carrying fine micritic carbonate sediment in suspension flows in a film down the side of the stalagmite. Some may be primary, fine-grained calcite, but we cannot preclude that some may be amorphous calcium carbonate, or fine-grained ikaite. However in the ripple laminae, no evidence of recrystallisation (e.g. pseudomorphs or moulds which are evidenced in the central column) was observed. The calcite accretion along the sides of the stalagmite therefore reflects a combination of agglomeration of this suspended material, together with rapidly precipitated additional calcite from this actively flowing film of alkaline water on the meniscus surface, as it continues to react with the CO_2 in the tunnel atmosphere.

Some of the fine lamination may also result from the precipitation of a fine layer of primary microcrystalline calcite as an “ice-like” crust on the surface of the film of water covering the top of the stalagmites. This is hypothesised to occur after the pH has decreased to the point where the solution is no longer saturated for ikaite. The formation of such a calcite film was directly observed occurring within a few minutes on dripwaters collected in petri dishes placed on top of actively-growing stalagmites. Slower calcite growth within the pore water beneath this surface, controlled by the diffusion of CO_2 through the surface film is consistent with the development of the micro-encrustations of coarser, euhedral calcite observed to have nucleated on microcrystals of calcite. Evidence of these features can be seen in the smaller stalagmite samples on the underside of each lamina and on the top surface of the preceding lamina (e.g. Figure 6(D-I)).

The findings at Peak Dale have implications for both the stability field for ikaite and the interpretation of pseudomorphs after ikaite. With regards the stability field, it is shown that ikaite can precipitate, and perfectly formed moulds of ikaite crystals can be preserved, at temperatures formerly believed to be above its maximum limit of stability. Calcite and aragonite pseudomorphs after ikaite and referred to variously as ‘thinolites’, ‘jarrowite’ or ‘glendonite’ within the literature (e.g. Bischoff et al., 1993; Shaikh and Shearman, 1987; Shearman and Smith, 1985) can be difficult to reconcile with ikaite’s monoclinic crystallography (Hesse and Kuppers, 1983). This may be due in part to ikaite’s instability: thus it is more common for these pseudo-crystals to be preserved in a subhedral rather than euhedral state, and the actual morphology reported may be a question of the scale at which observations are made. The literature widely discusses glendonites etc. as pseudomorphs after ikaite, when the ikaite dissolved millions of years ago. These pseudomorphs are accepted due to modern examples having a general spire-like, or needle morphology. On rare occasions when fresh ikaite can be examined with detailed microscopy, these spires can be seen to comprise of aggregates of numerous, fine-grained, euhedral crystals of ikaite which show monoclinic morphology. This is observed, for example, at Harpur Hill where micrometer-scale, euhedral ikaite crystals aggregate in complex dendritic spires on the mm scale (Mildowdowski et al., 2013), and it is

seems likely that it is the morphology of these mm-scale, dendritic spires that may be preserved as 'glendonites' etc. (see Figure 9, G, H and I). Recent experimental work by Sánchez-Pastor et al., (2016) has also produced micron-scale euhedral crystals with the same morphology as shown in Figure 9A and D.

The larger scale pseudomorphs have been used to infer cold-climate origins such as glacial or periglacial conditions (e.g. De Lurio and Frakes, 1999; Shearman and Smith, 1985). The well-preserved moulds within the Peak Dale speleothem have clearly formed within current warmer, Holocene climatic conditions, indicating that if conditions are favourable, and a high pH groundwater is present, ikaite formation is not limited solely to cold climate conditions.

Notable variations in morphologies between the short and tall Peak Dale stalagmites are, for the large part, likely to be related to whether or not the stalagmite has emerged above the maximum flooding level. The crystals within the smaller speleothem are interpreted as primary $CaCO_3$ (calcite dominated): no evidence for an ikaite precursor was identified. The smaller speleothem displaying only simple sub-horizontal lamination (MPLT635 and 636) are submerged for the majority of the year, only having limited periods for growth when the water level in the tunnel drops sufficiently to expose these stalagmites sub-aerially. Consequently the growth surface is only exposed when humidity levels are fractionally lower and drip rates at their most limited, resulting in a lack of excess dripwaters flowing down the side of the stalagmite and thus a lack of vertical ripple growth. The limited growth period coupled with slower, more restricted drip-rate during drier periods must have had an effect on the growth kinetics on these two samples. In addition, neither sample was in-situ when sampled, so an age relationship to the larger, intact and cryo-sample is not known. It is possible that these smaller speleothem may pre-date the other samples, and therefore it is possible that environmental conditions may have varied slightly to the current day, e.g. dripwaters may have had a lower pH than the current day, closer to pH 9.

Summary

Unusual and rapid-growing speleothem are being formed from shallow hyperalkaline calcium hydroxide type groundwater derived through the leaching of lime waste on the surface above the disused railway tunnel at Peak Dale. In contrast to the more commonly forming speleothems deposited from calcium bicarbonate groundwater following degassing of CO_2, the Peak Dale speleothems are formed by calcium carbonate precipitated as a result of the adsorption and reaction of atmospheric CO_2 with the calcium hydroxide water.

Unusual euhedral moulds that have been identified within the stalagmites are considered to have formed from ikaite, which initially precipitated from these hyperalkaline (pH 12.2-12.6) waters under the consistently cool (8.5 °C) conditions maintained within the tunnel. Although we conclude that ikaite initially forms, it is inferred to dissolve rapidly, followed by rapid or contemporaneous calcite precipitation, as the pH of the Ca^{2+}-OH^{-} type dripwater rapidly decreases through the adsorption and reaction with atmospheric CO_2. The transformation from ikaite to calcite is accompanied by a 68% decrease in molar volume, which would account for the development of a highly porous micro-fabric within these speleothem deposits. Although these are the first speleothem identified which contain ikaite moulds, it is likely that other examples exist within hyperalkaline environments.

Findings from Peak Dale, and the recently observed ikaite formation at nearby Harpur Hill (Milodowski et al., 2014 and 2013) both in Derbyshire, UK, suggest that under certain conditions, ikaite can grow and form euhedral crystals at temperatures above 6 ^{o}C.

Acknowledgements

The authors are grateful to Coke Turner and Co., Land Agents for the Duchy of Lancaster, for granting permission to work and sample within the tunnel, and Mr D. Abraham of Natural England for permission to access the tunnel entrance via the SSSI area. We thank John Fletcher of BGS for

making the thin sections. Gemma Purser and Lauren Selby assisted with field sampling of groundwaters. The Inorganic Geochemistry laboratories at the BGS, Keyworth carried out the analysis of the water samples. This paper is published with the permission of the Executive Director of the British Geological Survey (NERC). This research was funded under the Climate and Landscape Change research programme of the British Geological Survey. We gratefully acknowledge the reviews of Ian Fairchild and an anonymous reviewer which greatly improved the manuscript.

References

Allison, V.C., 1923. The growth of stalagmites and stalactites. Journal of Geology, **31**(2): 106-125.

Baker, A. et al., 1998. Testing Theoretically Predicted Stalagmite Growth Rate with Recent Annually Laminated Samples: Implications for Past Stalagmite Deposition. Geochimica et Cosmochimica Acta, **62**(3): 393-404.

Baker, A., Proctor, C.J., Barnes, W.L., 1999. Variations in stalagmite luminescence laminae structure at Poole's Cavern, England, AD 1910±1996: calibration of a palaeoprecipitation proxy. The Holocene, **9**(6): 683-688.

Baker, A., Smith, C.L., Jex, C., Fairchild, I.J., Genty, D., Fuller, L., 2008. Annually laminated speleothems: a review. International journal of speleology, **37**(3): 193-206.

Banks, V.J., Gunn, J., Lowe, D.J., 2009. Stratigraphical influences on the limestone hydrogeology of the Wye catchment, Derbyshire. Quarterly Journal of Engineering Geology and Hydrogeology, 42: 211-225.

Barnes, I., Presser, T.S., Saines, M., Dickson, P., Van Groos, A.F.K., 1982. Geochemistry of highly basic calcium hydroxide groundwater in Jordan. Chemical Geology, **35**(1–2): 147-154.

Bischoff, J.L., Fitzpatrick, J.A., Rosenbauer, R.J., 1993. The solubility and stabilization of ikaite ($CaCO_3.6H_2O$) from 0° to 25°C: Environmental and paleoclimatic implications for thinolite tufa. Journal of Geology, **101**(1): 21-33.

Boch, R., Dietzel, M., Reichl, P., Leis, A., Baldermann, A., Mittermayer, F., Pölt, P. 2015. Rapid ikaite ($CaCO_3$•$6H_2O$) crystallisation in a man-made river bed: Hydrogeochemical monitoring of a rarely documented mineral formation. Applied geochemistry, **63**: 366-379

Brunauer, S., Emmett, P.H., Teller, E., 1938. Adsorption of Gases in Multimolecular Layers. Journal of the American Chemical Society. **60**(2) 309–319, doi:10.1021/ja01269a023

Buchardt, B. et al., 1997. Submarine columns of ikaite tufa. Nature, 390: 129-130.

Dahl, K.; Buchardt, B., 2006. Monohydrocalcite in the arctic Ikka Fjord, SW Greenland: First reported marine occurrence. Journal of Sedimentary Research, **76**(3): 460–471. doi:10.2110/jsr.2006.035.

De Lurio, J.L., Frakes, L.A., 1999. Glendonites as a paleoenvironmental tool: implications for early Cretaceous high latitude climates in Australia. Geochimica et Cosmochimica Acta, **63**(7–8): 1039-1048.

Fairchild, I.J., Baker, A., 2012. Speleothem Science: From process to past environments. Wiley-Blackwell.

Frisia, S., Borsato, A., Fairchild, I.J., McDermott, F., Selmo, E.M., 2002. Aragonite-calcite relationships in speleothems (Grotte de Clamouse, France): Enironment, fabrics and carbonate geochemistry. Journal of Sedimentary Research, **72**(5): 687 - 699

Gagen, P.J., 1988. The evolution of quarried limestone rock slopes in the English Peak District. Unpublished PhD Thesis, CNAA at Manchester Polytechnic.

Gagen, P.J., Gunn, J. (Eds.), 1988. A geomorphological approach to limestone quarry restoration Geomorphology in environmental planning, . John Wiley and Sons, New York, pp 121-142p.

Gaines, R.V., Skinner, C.W., Foord, E.E., Mason, B., Rosenzweig, A. 1997. Dana's New Mineralogy: the system of mineralogy of James Dwight and Edward Salisbury, 8th ed. Wiley, New York, pp 1872

Hansen, M.O., Buchardt, B., Kühl, M., Elberling, B., 2011. The Fate of the Submarine Ikaite Tufa Columns in Southwest Greenland Under Changing Climate Conditions. Journal of Sedimentary Research, **81**(8): 553-561.

Hartland, A. et al., 2010. The dripwaters and speleothems of Poole's Cavern: a review of recent and ongoing research. Cave and Karst Science, **36**(2): 37 - 46.

Hesse, K.F., Kuppers, H., 1983. Refinement of the structure of Ikaite, CaC03 . 6 H20. Zeitschrift fUr Kristallographie, **163**: 227-231.

House, W.A., 1987. Inhibition of calcite crystal growth by inorganic phosphate. Journal of Colloid and Interface Science, **119**: 505-511.

Hu, Y.-B., Wolf-Gladrow, D.A., Dieckmann, G.S. Völker, C., Nehrke, G. 2014. A laboratory study of ikaite (CaCO3·6H2O) precipitation as a function of pH, salinity, temperature and phosphate concentration. Marine Chemistry, **162**, 10-18.

Ito, T., 1998. Factors controlling the transformation of natural ikaite from Shiowakka, Japan. Geochemical Journal, **32**: 267-273.

Liu, Z., He, D., 1998. Special speleothems in cement-grouting tunnels and their implications of the atmospheric CO_2 sink. Environmental Geology, **35**(4): 258-262.

Macleod, G., Fallick, A.E., Hall, A.J., 1991. The mechanism of carbonate growth on concrete structures, as elucidated by carbon and oxygen isotope analyses. Chemical Geology: Isotope Geoscience section, **86**(4): 335-343.

Marland, G., 1975. The stability of $CaCO_3 \cdot 6H_2O$ (ikaite). Geochimica et Cosmochimica Acta, **39**(1): 83-91.

McDermott, F., 2004. Palaeo-climate reconstruction from stable isotope variations in speleothems: a review. Quarternary Science Reviews, **23**: 901-918.

McMillan, E.A., Fairchild, I.J., Frisia, S., Borsato, A., McDermott, F., 2005. Annual trace element cycles in calcite-aragonite speleothems: evidence of drought in the western Mediterranean 1200 – 1100 yr BP. Journal of Quaternary Science, **20**(5): 423-433.

Milodowski, A., Rushton, J., Purser, G., Rochelle, C., Kemp, S., Shaw, R., Ellis, M., 2014. The Formation of Ikaite ($CaCO_3.6H_2O$) in Hyperalkaline Springs Associated with the Leaching of Lime Kiln Waste. Goldschmidt Abstracts, 1697. ISSN: 1042-7287.

Milodowski, A.E., Shaw, R.P., Stewart, D.I. 2013. The Harpur Hill Site: its geology, evolutionary history and a catalogue of materials present. *British Geological Survey Report*, CR/13/104. Available online at *https://rwm.nda.gov.uk/publication/harpur-hill-site-its-geology-evolutionary-history-and-a-catalogue-of-materials-present/*

Newton, K.E., Fairchild, I.J., Gunn, J. (2015). Rates of calcite precipitation from hyperalkaline waters, Poole's Cavern, Derbyshire, UK. Cave and Karst Science, **42**(3): 116-124

Omelon, C.R., Pollard, W.H., Marion, G.M., 2000. Seasonal formation of ikaite ($CaCO_3 \bullet 6H_2O$) in saline spring discharge at Expedition Fiord, Canadian High Arctic: Assessing conditional constraints for natural crystal growth. Geochimica et Cosmochimica Acta, **65**(9): 1429-1437.

Ordnance Survey data © Crown Copyright and database rights 2013. Ordnance Survey Licence No. 100021290

Parkhurst, D.L., Appelo, C.A.J., 2013. Description of input and examples for PHREEQC version 3 - A computer program for speciation, batch-reaction, one-dimensional transport, and inverse geochemical calculations. U.S. Geological Survey Techniques and Methods, **6**. USGS.

Pauly, H., 1963. "Ikaite", a New Mineral from Greenland. Arctic, **16**: 263-264.

Pinsent, B.R.W., Pearson, L., Roughton, F.J.W., 1956. The kinetics of combination of carbon dioxide with hydroxide ions. Transactions of the Faraday Society, **52**(0): 1512-1520.

Railsback, L.B., Brook, G.A., Chen, J., Kalin, R., Fleisher, C.J., 1994. Environmental controls on the petrology of a late Holocene speleothem from Botswana with annual layers of aragonite and calcite. Journal of Sedimentary Research A. **64**: 147-155

Roedder, E. 1968. The noncolloidal origin of "colloform" textures in sphalerite ores. Economic Geology **63**: 451-471.

Rodriguez-Blanco, J.D.; Shaw, S., Benning, L.G., 2011. The kinetics and mechanisms of amorphous calcium carbonate (ACC) crystallization to calcite, via vaterite. Nanoscale **3**: 265-271.

Rodriguez-Blanco, J.D., Shaw, S., Bots, P., Roncal-Herrero, T., Benning, L.G., 2014. The role of Mg in the crystallisation of monohydrocalcite. Geochimica et Cosmochimica Acta **127**: 204–220. doi:10.1016/j.gca.2013.11.034.

Sánchez-Pastor, N., Oehlerich, M., Astilleros, J.M., Kaliwoda, M., Mayr, C.C., Fernández-Díaz, L., Schmahl, W.W. 2016. Crystallization of ikaite and its pseudomorphic transformation into calcite: Ramen spectroscopy evidence. Geochimica et Cosmochimica Acta **175**: 271-281

Self, C.A., Hill, C.A., 2003. How speleothems grow: an introduction to the ontogeny of cave minerals. Journal of Cave and Karst Studies, **65**(2): 130-151.

Shaikh, A.M., Shearman, D.J., 1987. On ikaite and the morphology of its pseudomorphs. In: Rodriguez-Clemente, R., Tardy, Y. (Eds.), Geochemistry of the Earth Surface and Processes of Mineral Formation. Consejo Superior de Investigaciones Científicas Granada, Spain.

Shearman, D.J., McGugan, A., Stein, C., Smith, A.J., 1989. Ikaite, $CaCO_3.6H_2O$, precursor of the thinolites in the Quaternary tufas and tufa mounds of the Lahontan and Mono Lake Basins, western United States. Geological Society of America Bulletin, **101**(7): 913-917.

Shearman, D.J., Smith, A.J., 1985. Ikaite, the parent mineral of jarrowite-type pseudomorphs. Proceedings of the Geologists' Association, **96**(4): 305-314.

Spielhagen, R.F., Tripati, A., 2009. Evidence from Svalbard for near-freezing temperatures and climate oscillations in the Arctic during the Paleocene and Eocene. Palaeogeography, Palaeoclimatology, Palaeoecology , **278**: 48-56.

Sundqvist, H.S., Baker, A., Holmgren, K., 2005. Luminescence Variations in Fast-Growing Stalagmites from Uppsala, Sweden. Geografiska Annaler: Series A, Physical Geography, 87(4): 539-548.

Tucker, M. 2001. Sedimentary petrology: An introduction to the origin of sedimentary rocks. 3rd ed. Blackwell, Oxford.

Waters, C.N., Waters, R.A., Barclay, W.J., Davies, J., 2009. A lithostratigraphical framework for Carboniferous successions of Southern Great Britain (Onshore) RR/09/01, British Geological Survey, Keyworth, Nottingham.

UK Meteorological Office. MIDAS Land Surface Stations data (1853-current), [Internet]. NCAS British Atmospheric Data Centre, 2014. Available from: http://badc.nerc.ac.uk/view/badc.nerc.ac.uk__ATOM__dataent_ukmo-midas

Figure captions

Figure 1.

Location of tunnel. Map of tunnel overlain on an aerial photograph. (map of tunnel based on survey of R Eavis, J Gunn and K Eavis, 13th November 2013, Aerial photography ©UKP/Getmapping Licence No. UKP2006/01). Insert: map of the UK showing the Peak District area, and simplified map of the general locality of Peak Dale, with urban areas in black, M=Manchester, S=Sheffield, Ma=Macclesfield, B=Buxton.

Figure 2.

Images of the tunnel. A) View of the quarry wall with the location of tunnel entrance indicated by the arrow. Note the tunnel location between the houses of Small Knowle End. Quarry face ~9 m. B) General view of the tunnel from the entrance, showing an absence of speleothem within the initial 15 m of the tunnel and the speleothem-rich zone beyond. C) and D) showing the maximum and minimum water levels observed during 2013/2014 (C taken 1st March 2014 and D taken 3rd October 2014). The yellow rule (attached to the 3rd stalagmite from the left) is 1 m in length. E) The furthest point of the tunnel looking back towards the entrance. Beyond this point the tunnel is blocked, and this end is permanently flooded. This locality corresponds to the area directly beneath the road and

here the straw stalactites have a distinct brown colouration, possibly due to organic matter contamination.

Figure 3.

Graphs showing environmental conditions for 2014. Top, internal tunnel temperature compared to the external max and min temperatures for 26th Jan – 31st Dec 2014. External data from the British Meteorological Office returns (MIDAS) from Buxton (Station 539, ~5 km from the tunnel location). Bottom, daily precipitation at Buxton for the same period.

Figure 4.

Variation in chemistry of the alkaline stalactite dripwater in Peak Dale tunnel during 2014.

Figure 5.

Photographs of speleothem *in-situ*. A) image shows the frilly coating around the base of the speleothem which is related to secondary flood-level growth. B) Top of a speleothem showing side growth related to gravitational flow of unconsolidated solid calcium carbonate material and multiple drip points / excess dripping. These slippage planes can be identified in thin section, C) when drip rates are rapid, a 'splash cup' develops. This is preserved within the structure, and can be identified in the thin sections. D) View of a group of speleothems that display examples of the morphologies highlighted in A-C. These speleothem also demonstrate the corrugated texture along their length. The effect of migrating drips or periods when drips develop from multiple points in the tunnel roof are well evidenced in their structure.

Figure 6.

Morphology of the 'small' speleothem. A) Vertical slice through of the speleothem showing a generally horizontal laminated texture. B) Optical scanner image of part of a thin section showing pinching out of some laminae. C) Optical microscope image of the slice showing fine laminae. D)

BSEM image showing dense laminae interspersed with porous layers of upward growing crystals. D) SE image showing morphology of two dense laminae interspersed with a coarser, more porous layer. F) Detail of the crystals within the coarse layer in E. G) XPL image showing a crystal in extinction which extends across two laminae. H) and I) CCI images showing detail of complex zoning within the crystals. Note: The observations indicate these samples comprise primary $CaCO_3$ (calcite dominated): these speleothem lack the evidence of pseudomorphs and an ikaite precursor identified in the subsequent, larger samples.

Figure 7.

A) Slice of speleothem showing the central column of sub-horizontal laminae surrounded by vertically orientated asymmetrical ripples. B) Optical scanner image of the thin section clearly illustrating the two general morphologies. C) SE image of a series of asymmetrical ripples (side on view). D) BSEM thin section view of the ripples. E) SE image showing detail of a ripple comprising a series of outwardly growing crystals. F) BSEM thin section view of the colloform-type morphology. G) SE view of a colloform laminae in profile. H) SE cross-section view through an asymmetric ripple, showing colloform growth on the underside and outwardly growing, straight crystal growth on the upper surface.

Figure 8.

A) and B) SE and BSEM image respectively, of pseudomorphs after ikaite. Image A shows pseudomorphs that have been coated with resin; these forms are defined by an aggregate of numerous fine-grained calcite crystals (<10 μm). These small calcite crystals are visible above the level of the resin. Image B shows the hollow nature of the pseudomorphs. C) SE image showing partial pseudomorph moulds. The interior is hollow, whilst the pseudomorph is defined by calcite crystals (<1 μm). D) SE image of the calcite aggregate defining the pseudomorph outer-coating (individual calcite crystals <10 μm). E) BSEM image detail of a pseudomorph outline in thin section.

F) and G) detail showing the skeletal nature of the individual calcite crystals which collectively define the pseudomorphs. H) and I) ESEM images from the cryogenic sample of these fine grained calcite crystals. H) Euhedral calcite overgrowth tips above secondary calcite. I) Horizontal section through an individual calcite crystal showing fresh overgrowth around a 'cabbage leaf', skeletal interior, now entirely comprising calcite.

Figure 9.

Comparison of moulds from the non-in situ sample (A), and the intact sample (thin section: B, C), the 'cryogenic' sample (E and F), alongside fresh ikaite crystals (confirmed by XRD analysis: Milodowski et al., 2013, 2014) from Harpur Hill (D, G, H and I). Note the close similarities between the pseudomorphed crystal form of the Peak Dale speleothem material, and actual ikaite forming at Harpur Hill (compare (A) to (D) which show a monoclinic symmetry which cannot be assigned to calcite, and (E and F) to (I)). The faces labelled 'a' in (I) relate to those shown in (E) and (F), and the faces labelled b in (I) relate to (D) and (G). Note that these fine-grained, complex, euhedral crystals (<200 μm: D and G) aggregate into complex, dendritic spires. These aggregates are akin to the 'glendonite' and 'jarrowite' pseudomorphs after ikaite, more commonly preserved in the geological record.

Figure 10.

XRD trace obtained from a frozen, powdered sample, washed in methanol and analysed at -20 ^{o}C in a cryogenic chamber on a PANalytical X'Pert Pro diffractometer. Several repeat analyses from different parts of the speleothem produced almost identical results. Standard 'stick' patterns for calcite (~99%) and trace quartz (<1%) are shown.

Figure 11.

Nitrogen sorption isotherms for inner and outer column samples, analysed from 0.01 - 0.99 p/po at -196 °C. Solid lines denote adsorption curve, dashed line denote desorption curve.

Figure 12.

MIP profiles for inner and outer columns, analysed from 0.5 to 60,000 psi.

Figure 13.

Cartoon of the proposed ikaite precipitation / destabilisation process. A) High pH, Ca^{2+}-OH^{-} dominated dripwaters drip from the feeder straws onto the stalagmite. B) In this air-dominated system, CO_2 is sequestered from the tunnel environment into the film of dripwater on the surface of the stalagmite. C) The high pH stabilises ikaite which rapidly precipitates from the dripwaters. As ikaite precipitates, this causes the pH of the dripwaters to fall. D) The fall in pH causes the ikaite to begin to destabilise, and fine-grained calcite contemporaneously nucleates on the surface of the ikaite crystals. This replacement results in a 68% volume reduction. Finally, all ikaite destabilises leaving fine-grained $CaCO_3$ which defines the mouldic cavities left by the precursor ikaite, and free H_2O. This process constantly repeats with each new high pH drip.

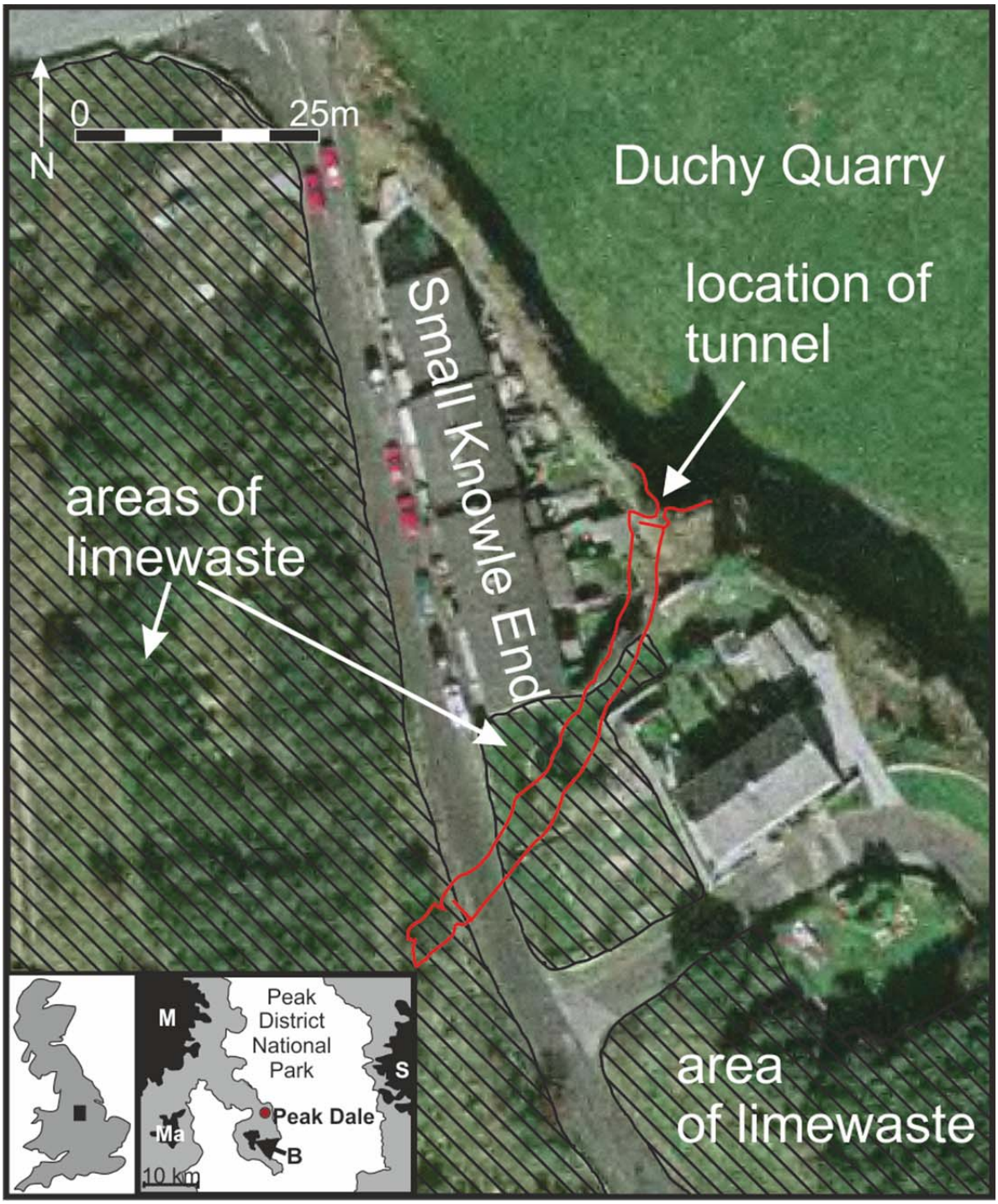
N
0
25m
Duchy Quarry
location of tunnel
Small Knowle End
areas of limewaste
area of limewaste
Peak District National Park
M
S
Peak Dale
B
10 km

Figure 1.

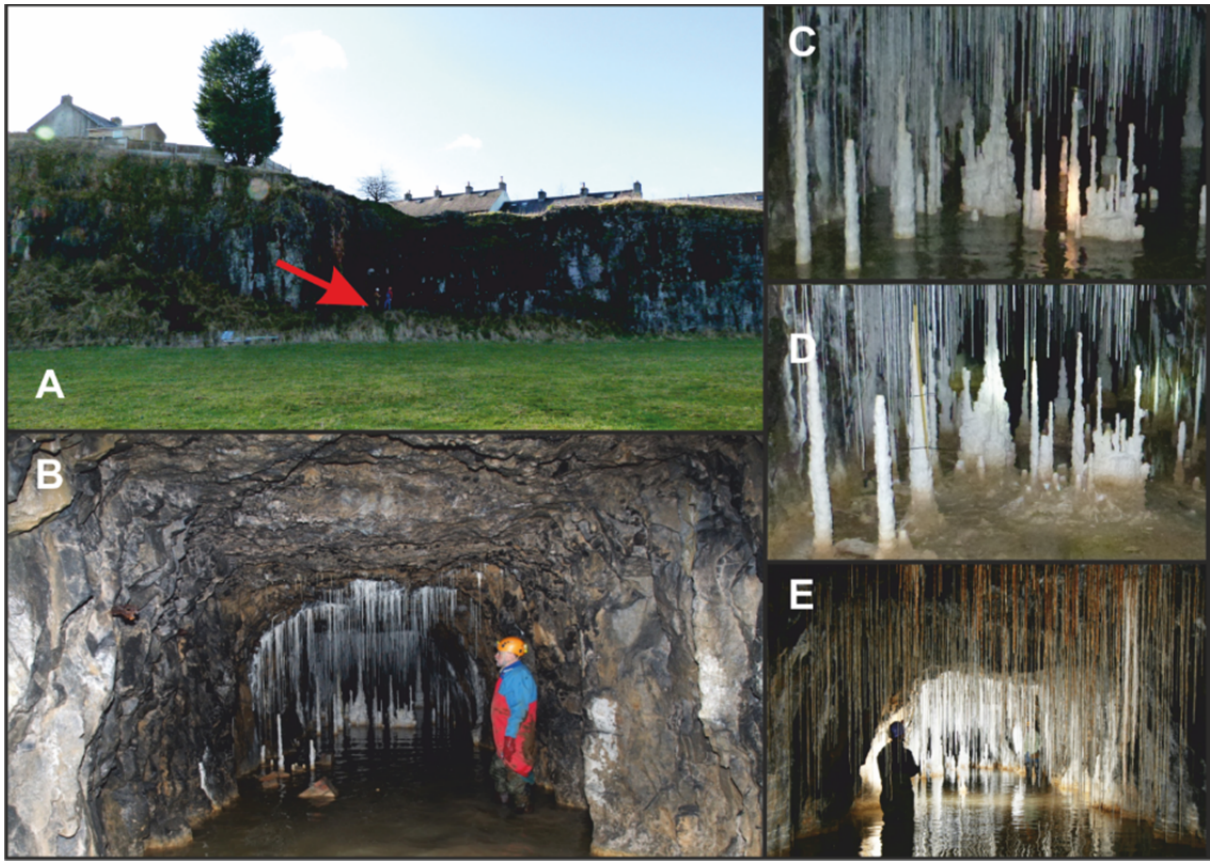

Figure 2.

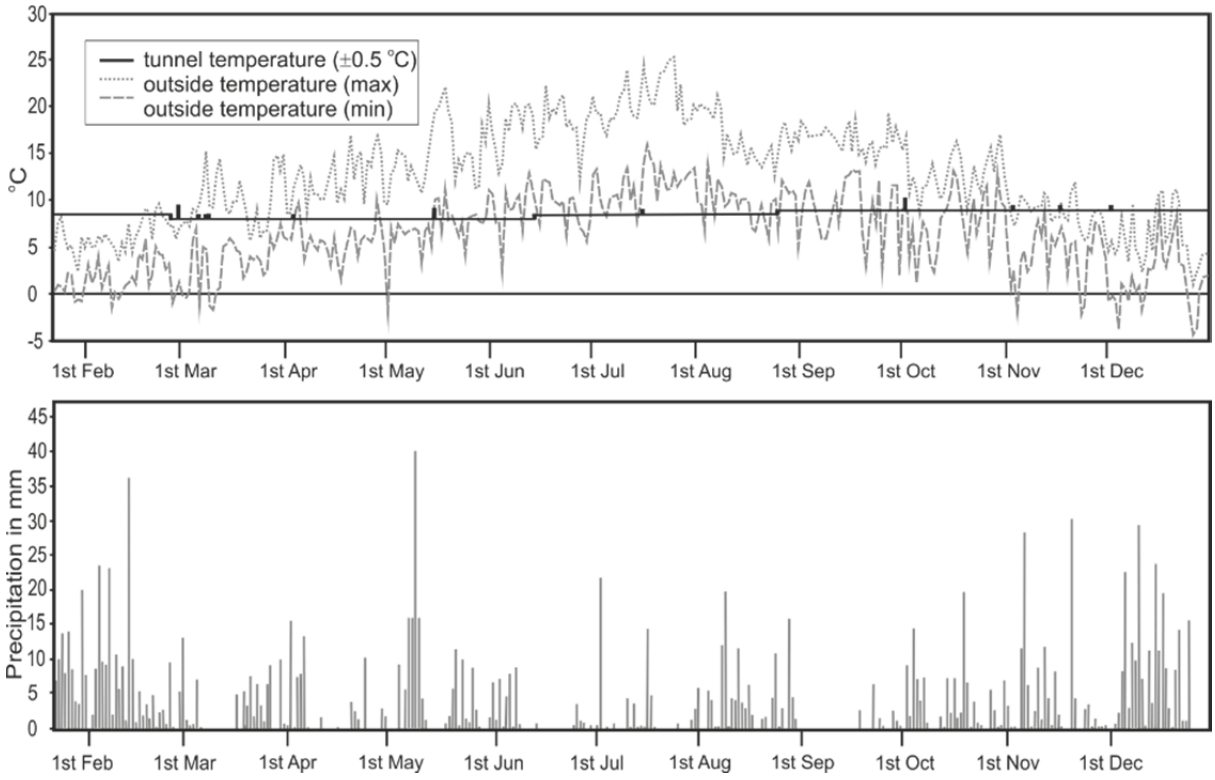
tunnel temperature (±0.5 °C)
outside temperature (max)
outside temperature (min)
°C
30
25
20
15
10
5
0
-5
1st Feb
1st Mar
1st Apr
1st May
1st Jun
1st Jul
1st Aug
1st Sep
1st Oct
1st Nov
1st Dec
Precipitation in mm
45
40
35
30
25
20
15
10
5
0
1st Feb
1st Mar
1st Apr
1st May
1st Jun
1st Jul
1st Aug
1st Sep
1st Oct
1st Nov
1st Dec

Figure 3.

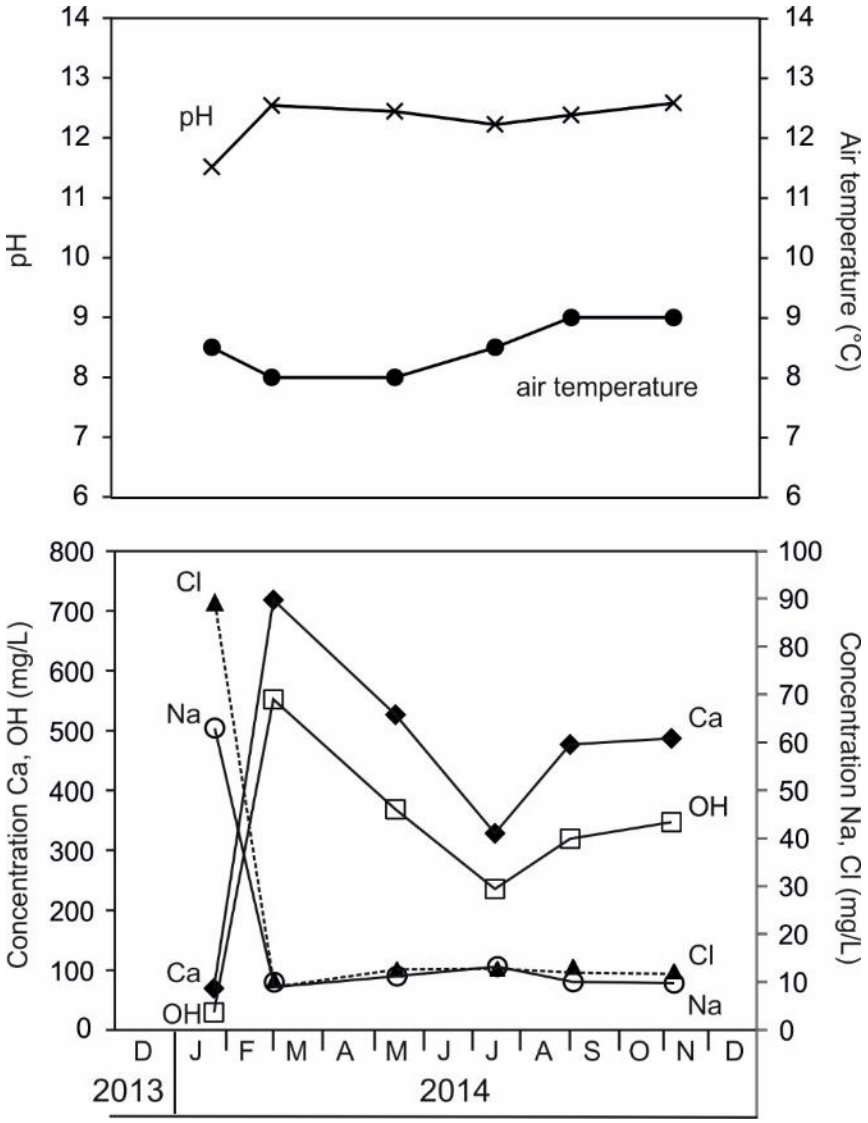
pH
air temperature
pH
Air temperature (°C)
Cl
Na
Ca
OH
Concentration Ca, OH (mg/L)
Concentration Na, Cl (mg/L)
D J F M A M J J A S O N D
2013
2014

Figure 4.

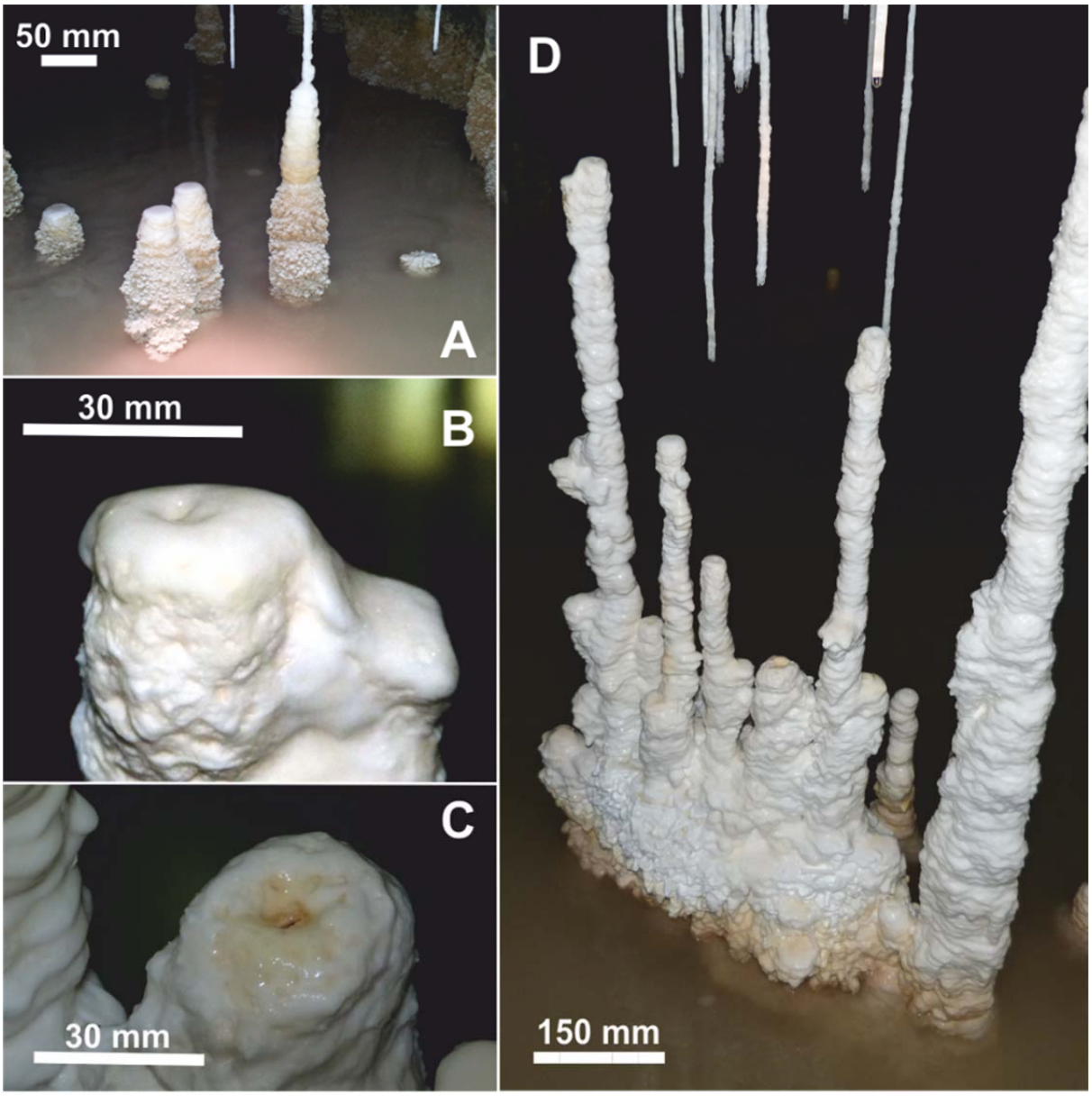

Figure 5.

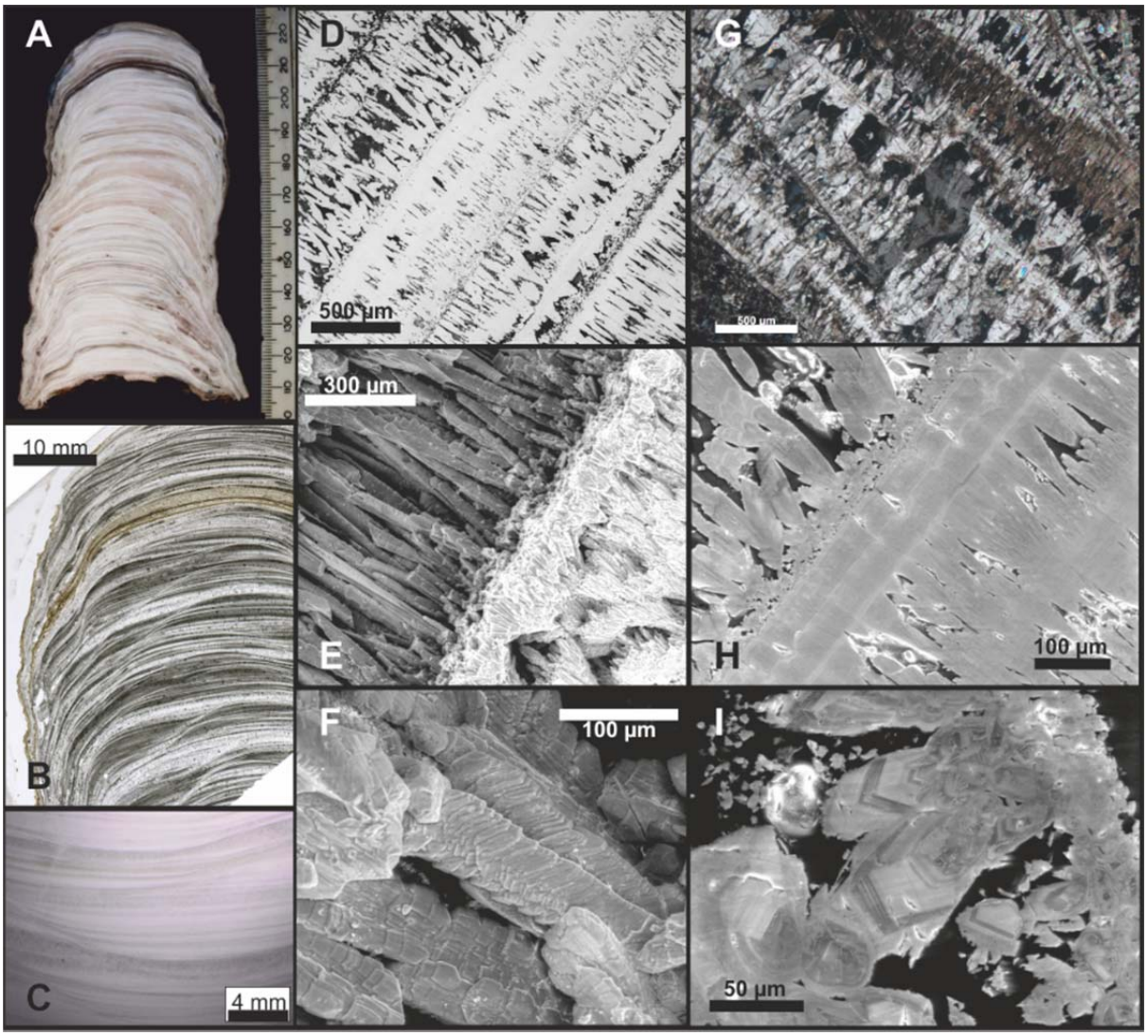

Figure 6.

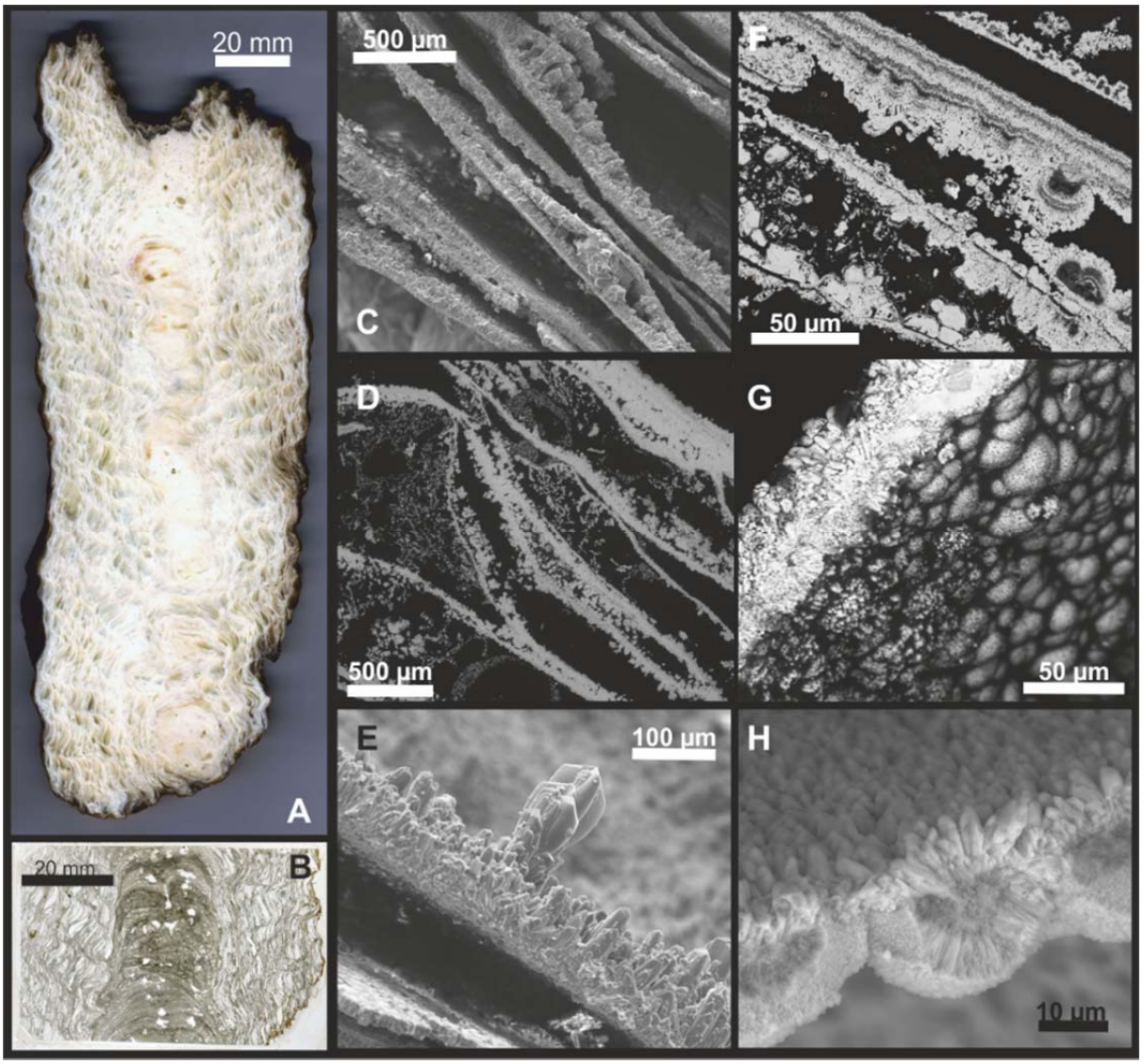

Figure 7.

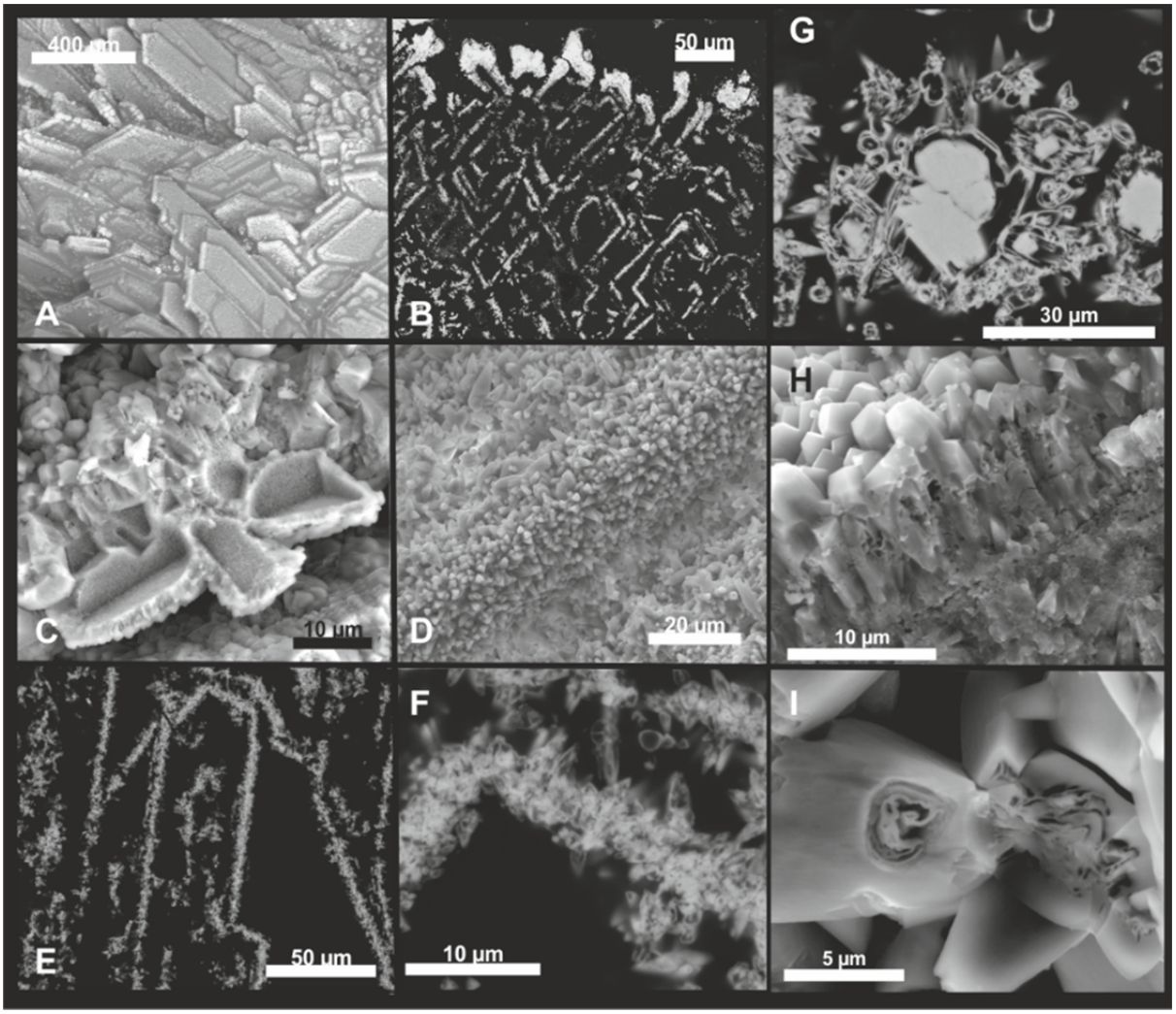

Figure 8.

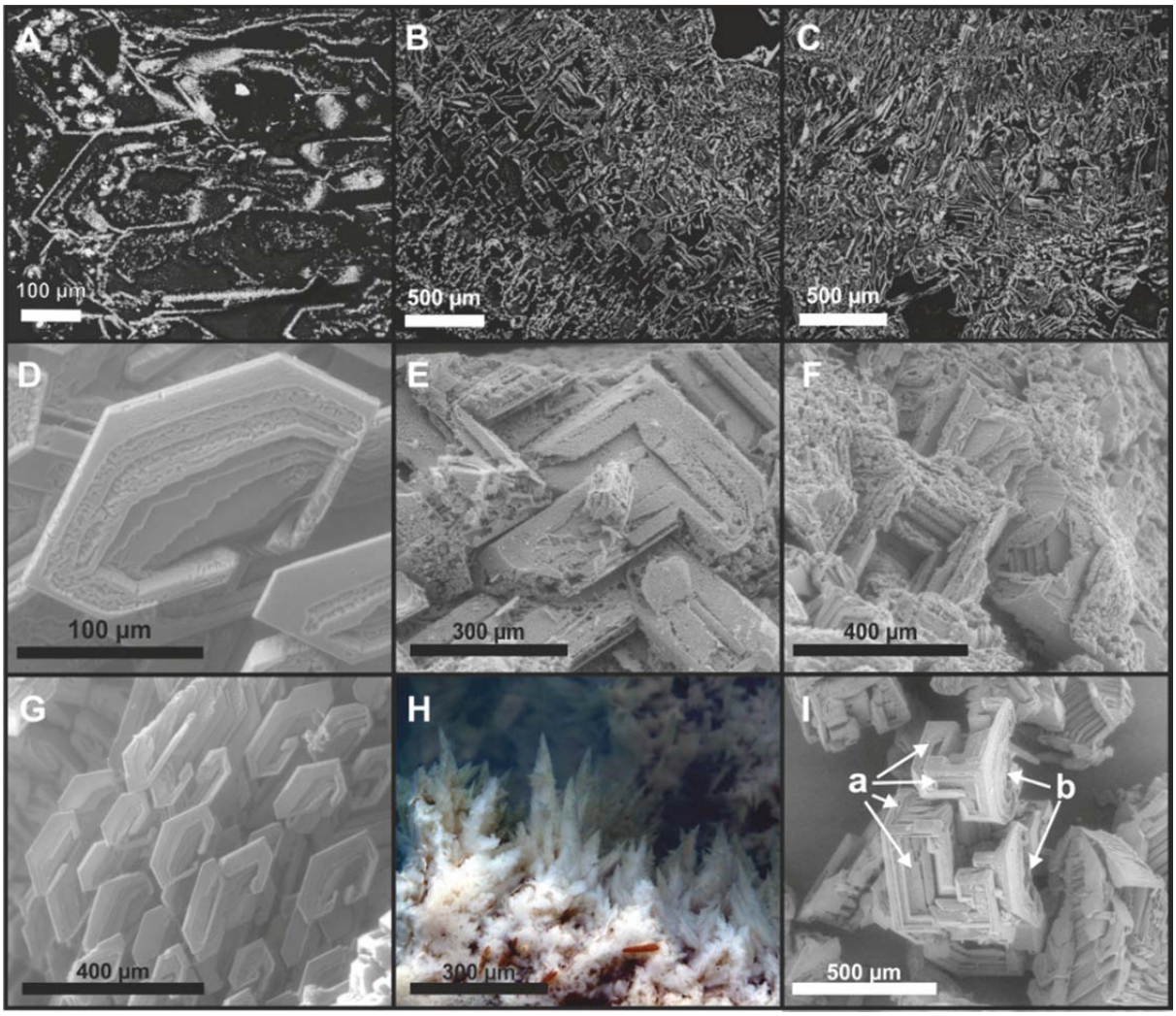
A
100 µm
B
500 µm
C
500 µm
D
100 µm
E
300 µm
F
400 µm
G
400 µm
H
300 µm
I
a
b
500 µm

Figure 9.

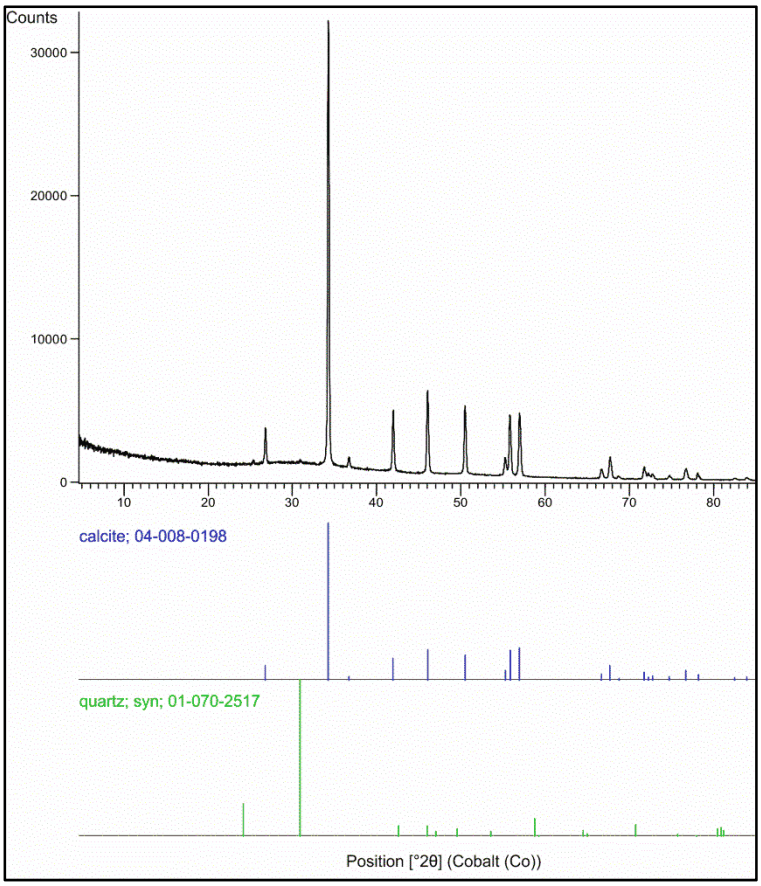
Counts
30000
20000
10000
0
10
20
30
40
50
60
70
80
calcite; 04-008-0198
quartz; syn; 01-070-2517
Position [°2θ] (Cobalt (Co))

Figure 10.

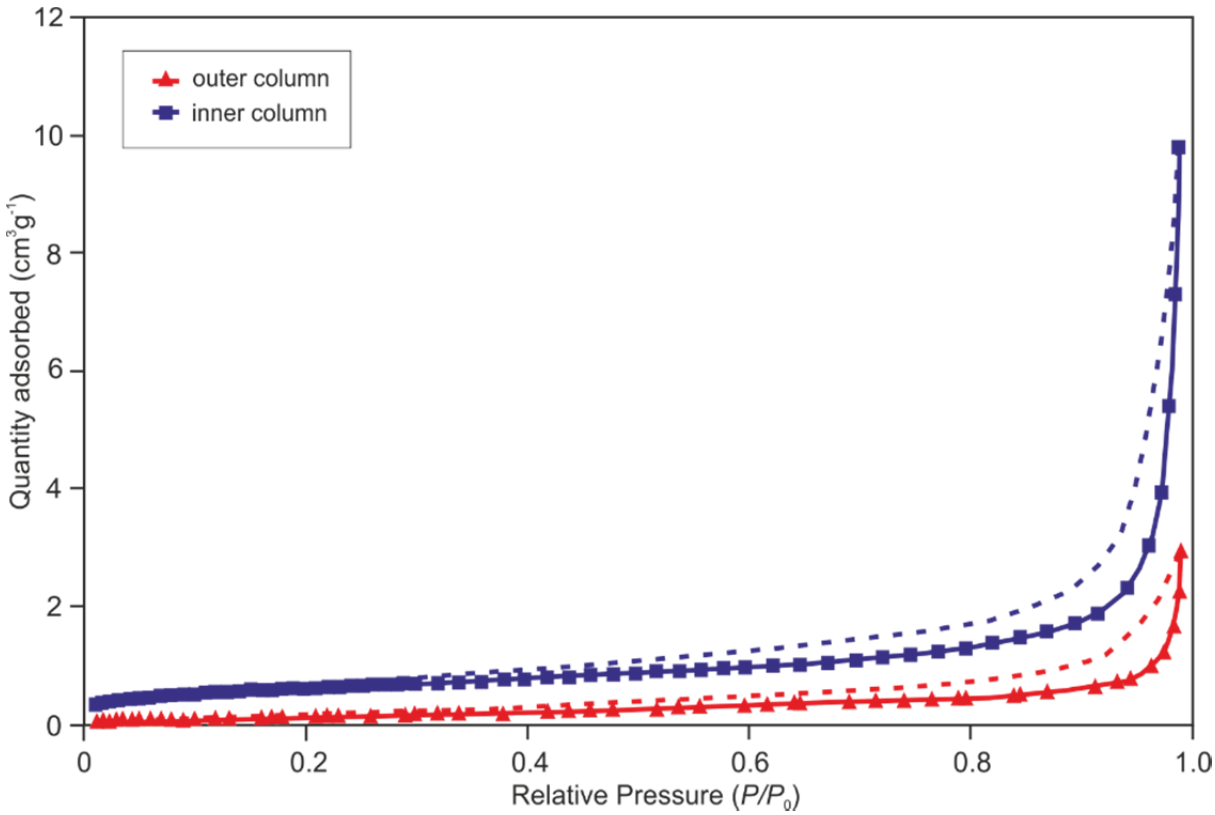
outer column
inner column
Quantity adsorbed (cm³g⁻¹)
Relative Pressure (P/P0)
0
2
4
6
8
10
12
0
0.2
0.4
0.6
0.8
1.0

Figure 11.

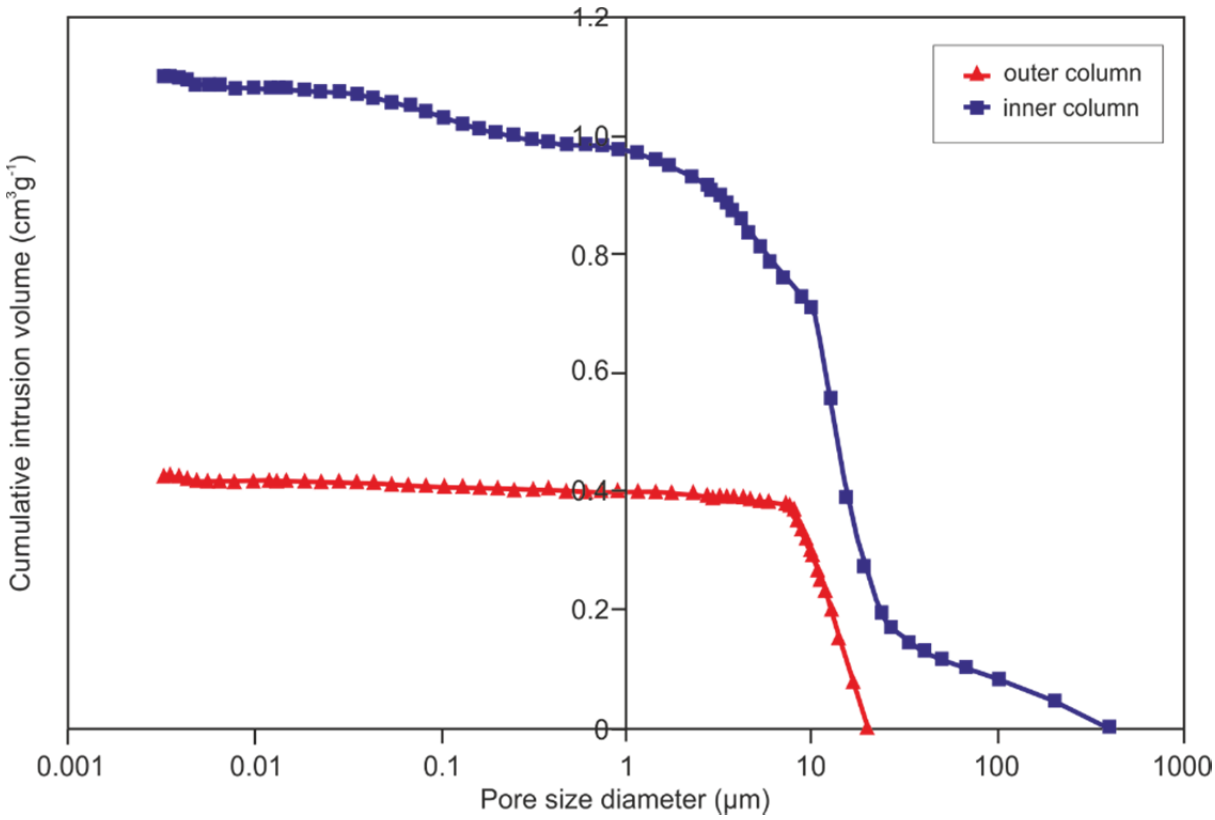
outer column
inner column
Cumulative intrusion volume (cm³g⁻¹)
1.2
1.0
0.8
0.6
0.4
0.2
0
0.001
0.01
0.1
1
10
100
1000
Pore size diameter (μm)

Figure 12.

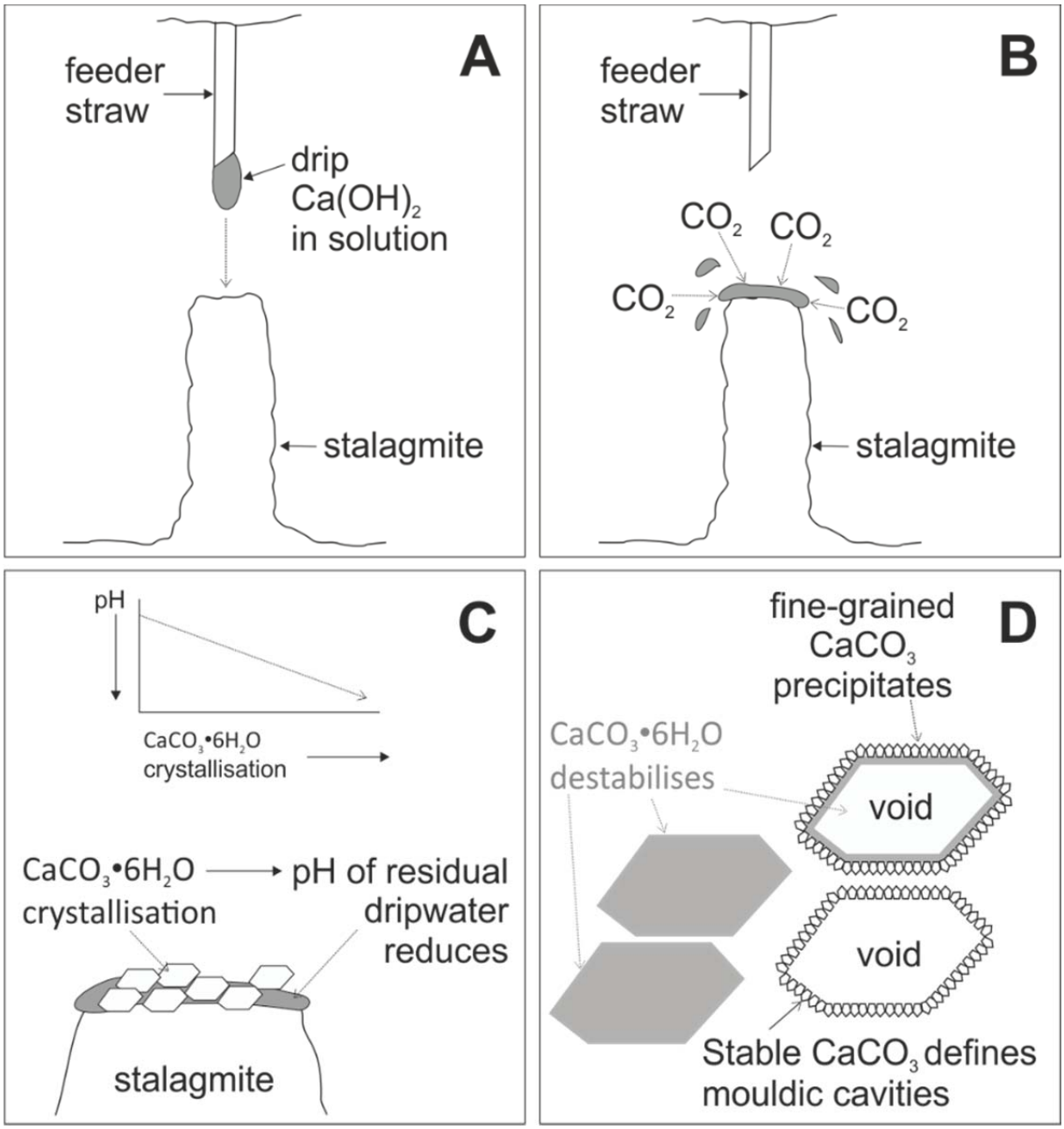
A
feeder straw
drip $Ca(OH)_2$ in solution
stalagmite
B
feeder straw
CO_2
CO_2
CO_2
CO_2
stalagmite
C
pH
$CaCO_3 \cdot 6H_2O$ crystallisation
$CaCO_3 \cdot 6H_2O$ crystallisation
pH of residual dripwater reduces
stalagmite
D
fine-grained $CaCO_3$ precipitates
$CaCO_3 \cdot 6H_2O$ destabilises
void
void
Stable $CaCO_3$ defines mouldic cavities

Figure 13.

Table 1: Variation over the year in the chemistry of drip water associated with the speleothem within the main hyperalkaline inflow zone

Date	23-Jan-14	01-Mar-14	16-May-14	17-Jul-14	02-Sep-14	04-Nov-14
T °C (Tunnel)	8.5	8	8	8.5	9	9
pH (field)	11.1	n.d.	12.5	n.d.	n.d.	12.8
T °C (lab)	18	18	18	18	18	18
pH (lab)	11.5	12.5	12.4	12.2	12.4	12.6
Conductivity (µS cm^{-1})	n.d.	6870	n.d.	3620	4790	4800
	mg L^{-1}					
Ca	69	718	526	328	476.3	486.6
Mg	0.24	<0.1	<0.1	<0.1	<0.1	<0.1
Na	62.8	9.7	11	13	9.8	9.5
K	10.8	14.5	20.2	24.1	23.8	23.4
OH^-	29	552	368	235	319	347
CO_3^{2-}	<15	-	24.4	13.2	24.7	19.2
HCO_3^-	-	-	-	-	-	-
Cl^-	89.1	10.1	12.4	12.5	12.9	12
SO_4^{2-}	49.7	66	32.3	24.6	22.4	23.2
NO_3^-	27.2	23	31.7	30.5	32.3	32.7
NO_2^-	0.37	0.25	0.53	0.82	0.99	0.85
F^-	0.09	<0.05	0.17	<0.01	<0.01	<0.01
NPOC	2.22	3.81	n.d.	4.16	4.91	n.d.
Si	3	0.14	0.09	<0.07	0.08	0.06
	µg L^{-1}					
Al	361	11	17	10	21	8
Ba	29.1	178	198	151	203	205
Sr	101	387	392	364	453	433
Fe	6	11	<4.0	21	23	6

Notes: n.d. = not determined in the field. P, Br^- and Mn also measured but all measurements were below detection (<0.05 and <0.1 mg L^{-1}, and, <1.0 µg L^{-1} respectively).

Table 2. Incorporating textural properties from MIP and nitrogen sorption isotherms spanning the micro-, meso- and macro pore range. a denotes data from MIP with bulk density determined at 0.50 psi, and apparent skeletal density at 60,000 psi. % porosity calculated by (1 – (Bulk/Skeletal)), b denotes data acquired from nitrogen sorption isotherms.

Sample	Total intrusion volume[a] (cm3 g-1)	Total pore area[a] ($m^2 g^{-1}$)	Density[a] (gcm^{-3})		% Porosity[a]	BET surface area[b] ($m^2 g^{-1}$)	BET 'C'[b]	Total pore volume[b] ($cm^3 g^{-1}$)
			Bulk	Apparent skeletal				
Inner	1.10	21.84	0.58	1.59	64	2.26	108	0.02
Outer	0.40	8.43	1.14	2.21	48	0.53	20	0.01

Table 3. Intrusion or pore volume associated with a specific pore diameter size range from MIP.

Sample	Total intrusion / pore volume ($cm^3 g^{-1}$)	Pore volume per size range ($cm^3 g^{-1}$)						
		390 – 25 µm	25 – 10 µm	10 – 4 µm	4.0 – 0.7 µm	0.700 – 0.165 µm	0.165 – 0.050 µm	0.050 – 0.003 µm
Inner	1.10	0.18	0.53	0.16	0.12	0.03	0.05	0.04
Outer	0.40	0	0.29	0.07	0.01	0.01	0.01	0.01

Table 4. Summary of dripwater modelling results

Date	23-Jan-14	01-Mar-14	16-May-14	17-Jul-14	02-Sep-14	04-Nov-14
T °C (Tunnel)	8.5	8	8	8.5	9	9
pH (field)	11.11	n.d.	12.49	n.d.	n.d,	12.79
pH (lab)	11.51	12.54	12.44	12.22	12.38	12.58
Initial Fluid pH (PHREEQC)	11.71	12.93	12.78	12.6	12.69	12.72
pH following equilibration with atmospheric CO_2 (PHREEQC)	5.5	10.6	9.2	7	8.7	9
Initial Ikaite SI*	-6.48	-6.29	0.31	0.01	0.28	0.17
Ikaite SI* following equilibration with CO_2**	-3.82	1.87	1.39	-0.8	0.98	1.22
Initial Calcite SI*	-5.04	-4.86	1.74	1.45	1.74	1.63
Calcite SI following equilibration with CO_2**	-2.38	3.29	2.81	0.65	2.44	2.68
Initial Portlandite ($Ca(OH)_2$) SI	-3.4	-0.33	-0.7	-1.14	-0.8	-0.73
Portlandite ($Ca(OH)_2$) SI following CO_2 eq.**	-15.87	-5.25	-7.82	-12.17	-8.71	-8.11

Notes: *Saturation index (SI) values for calcite and ikaite have been calculated in PHREEQC (Parkhurst and Appelo 2013), using the Lawrence Livermore National Laboratory thermodynamic database (LLNL data). LogK data for ikaite was taken from Bischoff et al. (1993), but it should be noted that this is a very limited single dataset. **CO_2 partial pressure = 0.0004 atm)